PARAMETERIZATION OF THE CRYSTAL STRUCTURES OF CENTROSYMMETRIC ZONE-BOUNDARY-TILTED PEROVSKITES: AN ANALYSIS IN TERMS OF SYMMETRY-ADAPTED BASIS-VECTORS OF THE CUBIC ARISTOTYPE PHASE

Kevin S. KNIGHT[§]

ISIS Facility, Rutherford Appleton Laboratory, Chilton, Didcot, Oxfordshire, OX11 0QX,
and Department of Mineralogy, The Natural History Museum, Cromwell Road, London, SW7 5BD, United Kingdom

ABSTRACT

The methods of group theory have been used to decompose the crystal structures of centrosymmetric perovskites, ABX_3, that exhibit zone-boundary tilting of the BX_6 octahedra. For the fourteen space-groups consistent with these phenomena, the associated structures are decomposed in terms of the magnitudes of an appropriate set of symmetry-adapted basis-vectors of the primitive cubic aristotype phase of perovskite at high-symmetry points on the surface of the Brillouin zone. The advantage of this parameterization is twofold; firstly, octahedron tilt angles can be determined precisely and independently of the effects of octahedron distortion, and secondly, the degrees of freedom required by the perovskite structure can be rigorously derived. The method is outlined using the results of a neutron-diffraction investigation of $CaTiO_3$ in space group *Pbnm*, an example where the structural degrees of freedom are found to be one less than that required by the space group. Full results that can be very simply utilised in the decomposition of the other thirteen space-groups are tabulated. The advantages of decomposing perovskite-structured phases in this way are further illustrated using the temperature dependence of the crystal structure of $KCaF_3$ between 4.2 and 542 K.

Keywords: perovskite, crystal structure, group theory.

SOMMAIRE

Les méthodes de la théorie des groupes ont été utilisées afin de décomposer les structures cristallines des pérovskites centrosymétriques, ABX_3, qui font preuve d'inclinaison d'octaèdres BX_6 en bordure de zones. Pous les quatorze groupes spatiaux qui peuvent subir ces phénomènes, les structures associées sont décomposées en termes de l'amplitude d'un ensemble approprié de vecteurs fondamentaux pour décrire la pérovskite primitive cubique, la phase aristotype, adaptés à la symétrie réelle, telle que déterminée à des points de symétrie élevée sur la surface de la zone de Brillouin. Il y a deux avantages de ce paramétrage: premièrement, les angles d'inclinaison des octaèdres peuvent être déterminés avec précision et indépendamment des effets dus à la distortion des octaèdres; deuxièmement, on peut en dériver rigoureusement les degrés de liberté requis par la structure de la pérovskite. On décrit cette méthode en utilisant les résultats d'une étude de $CaTiO_3$ dans le groupe spatial *Pbnm* par diffraction de neutrons, un exemple dans lequel les degrés de liberté sont un de moins que ceux requis par le groupe spatial. Les résultats complets présentés dans les tableaux peuvent être très facilement utilisés dans la décomposition des treize autres groupes spatiaux. Les avantages d'une décomposition de phases ayant la structure de la pérovskite sont aussi illustrés en examinant la dépendance de la structure cristalline de $KCaF_3$, ayant la structure de la pérovskite, entre 4.2 et 542 K.

(Traduit par la Rédaction)

Mots-clés: pérovskite, structure cristalline, théorie des groupes.

[§] *E-mail address*: kevin.knight@stfc.ac.uk

INTRODUCTION

The rich structural diversity exhibited by the perovskite family and related compounds, including both cation-ordered phases and inorganic–organic hybrids, which have been recently reviewed in an excellent monograph by Mitchell (2002), presents significant challenges to the crystallographer. The aristotype phase of perovskite, ABX_3, has space group $Pm\overline{3}m$ with a large cation (A) in a dodecahedrally coordinated site in Wyckoff position 1b, a smaller, octahedrally coordinated cation (B) in position 1a, and three anions (X) in position 3d. Despite their chemical simplicity, the perovskite group of compounds and the structurally related, chemically ordered compounds, those of the elpasolite group, $A_2BB'X_6$, are crystallographically subtle. Both families generally show a strongly pseudocubic lattice metric that requires diffraction data collected at the highest possible resolution to be certain of the correct determination of the crystal system and space group. In addition to this requirement, the determination of the correct space-group for phases that exhibit tilting of the BX_6 and $B'X_6$ octahedra is generally further exacerbated by the anions being light, usually oxygen, but occasionally halogens, whereas the A- and B-site cations are usually significantly heavier atoms. If this is indeed the case, X-ray-diffraction data will appear to be quasi-I-centered on the pseudocubic subcell (subscripted p) owing to the approximate separation of the A and B sites by the pseudocubic vector $\frac{1}{2}(\mathbf{a_p} + \mathbf{b_p} + \mathbf{c_p})$, coupled with the weakness of the superlattice reflections that arise from the tilting of the octahedra. The importance of precisely characterizing these superlattice reflections has been emphasised by Glazer (1975) in a review of methods to reliably determine the crystal structures of perovskites. Neutron scattering lengths, unlike X-ray form factors, are neither dependent on atomic number,

nor on Q $(Q = \dfrac{4\pi\sin\vartheta}{\lambda}$, λ, wavelength, θ, half the

scattering angle). Hence in neutron-diffraction patterns, the quasi-I-centering of the diffraction pattern is less pronounced, and the intensities of the superlattice reflections may have magnitudes that are comparable with those of the fundamental reflections. Hence, provided that samples can be prepared in bulk form, this property has made neutron diffraction the technique of choice for the detailed crystallographic analysis of heavy-atom-bearing oxide systems.

Commensurate with the problems associated with pseudosymmetry is the presence of multiple twins in single crystals that have undergone ferroelastic phase-transitions on cooling from their temperature of synthesis. In the worst possible case, this can render single-crystal diffraction data difficult, if not impossible, to interpret; for example, in the case of the single-crystal data collected on $MgSiO_3$ at 400 K, it was not even possible to determine the lattice parameters because of the high density of twins (Ross & Hazen 1989). Neither of these problems is of serious consequence to data collected on state-of-the-art high-resolution neutron or synchrotron powder diffractometers. As many synthetic perovskite phases, if not most, are prepared by solid-state reaction, powder-diffraction techniques and the Rietveld method are generally employed to determine and refine the crystal structures of novel compounds. A discussion of the difficulty in characterizing polycrystalline perovskite-structured phases can be found in many places in the literature (Glazer 1975, Mitchell 2002), and the crystal structures of many compounds can be seen to "evolve in time" to the correct solution as improvements have been made in instrumental resolution and as alternative radiations become employed in data collection. Recent examples of cases where high instrumental resolution coupled with the intrinsic advantages of neutron diffraction have been used to resolve long-standing crystallographic ambiguities include the ambient-temperature crystal structure and the high-temperature phase transitions of the mixed-ion conductor, $BaCe_xRE_{1-x}O_{3-\delta}$ (RE: rare earth, Y) (Knight 1994, 2001), and the correct identification of the high-temperature phases in $SrZrO_3$ (Howard et al. 2000).

Once the correct space-group has been identified, and the crystal structure has been refined, it is necessary to interpret the physical properties or crystal-chemical parameters in terms of the observed structure. Despite the simplicity of the perovskite structure, the challenge of relating the structural distortions, manifested by changes in bond lengths and angles from the cations to the anions, to the physicochemical properties, is not always clearcut. In the work to be reported here, the crystal structures associated with the fourteen possible centrosymmetric space-groups consistent with tilting of the octahedra are parameterized in terms of a set of appropriate symmetry-adapted basis-vectors of the aristotype phase. To an excellent approximation, the displacements of the A-site cation and the anions can be written as linear combinations of the magnitudes (with sign) of an appropriate set of symmetry-adapted basis-vectors (sabvs) of the aristotype phase. In turn, the magnitudes of the sabvs, and estimates of their standard deviations, can be easily derived from the physical displacements and their estimated errors by the inverse process. Using results from powder neutron-diffraction studies, the simplicity and advantage of this decomposition are illustrated for two particular cases; the precise refinement of the crystal structure of $CaTiO_3$ at room temperature, and a detailed parametric study of the temperature dependence of the crystal structure of $KCaF_3$ in the $Pbnm$ phase.

An identical analysis for elpasolite-structured phases has already been carried and is published in this issue (Knight 2009).

REVIEW OF THE RELEVANT LITERATURE

In an investigation of the lattice dynamics of the cubic to tetragonal phase-transition in $SrTiO_3$, Cowley (1964) showed that rigid unit rotation (tilting) of the TiO_6 octahedron about <100> occurred for two zone-boundary phonons; at the M point of the cubic Brillouin zone ($\frac{1}{2}\mathbf{a^*} + \frac{1}{2}\mathbf{b^*}$) and symmetry-related points, with irreducible representation (*irrep*) M_3, and at the R point ($\frac{1}{2}\mathbf{a^*} + \frac{1}{2}\mathbf{b^*} + \frac{1}{2}\mathbf{c^*}$), with *irrep* Γ_{25}. In the Miller–Love notation (Bradley & Cracknell 1972), which has now become the standard used in all the recent group-theory studies of perovskites, these modes have the *irreps* M_3^+ and R_4^+, respectively. By using projection operator techniques, Cowley showed that the phonon with the *irrep* M_3^+ requires successive layers of octahedra to rotate in the same sense, whereas the phonon with the *irrep* R_4^+ requires successive layers of octahedra to rotate in the opposite sense. If either, or both, modes are soft and condense on cooling from high temperature, then a superlattice reflection will be observed at these points in reciprocal space. The weakness of these superlattice reflections when one uses X-ray-diffraction to characterize can hence be attributed to the fact that the displacements associated with these phonons only affect the anion and not the cation positions. In addition, for phases in which both the M point and the R point are reciprocal lattice vectors, then the vector between them is also a reciprocal lattice vector, this being the X point ($\frac{1}{2}\mathbf{c^*}$) of the pseudocubic Brillouin zone.

Systematic crystallographic classification of centrosymmetric perovskite-structured phases exhibiting these zone-boundary tilting modes was first published in a seminal paper by Glazer (1972), in which twenty-three independent tilt systems were recognized and their corresponding space-groups identified. Glazer characterized the two phonon-displacement patterns as either representing an in-phase tilt (M_3^+), or an anti-phase tilt (R_4^+), and described the possible patterns of tilting using a simple notation. The Glazer symbol ($a^\# b^\# c^\#$) for any space group summarizes the pattern of tilting in a particularly succinct manner; the literals represent the magnitudes of the tilts around the [100], [010] and [001] axes of the aristotype phase, whereas the superscripts (#), either +, – or 0, represent the nature of the tilt around that particular axis, + for an in-phase tilt, – for an anti-phase tilt, 0 for no tilt. Hence, $a^+a^+a^+$ represents the phase with three equal in-phase tilts (space group $Im\bar{3}$, whereas $a^-b^-c^+$ represents the phase with two anti-phase tilts of different magnitude and an in-phase tilt of a third magnitude (space group $P\,1\,1\,2_1/m$). In subsequent years, the original results determined by Glazer have undergone many reappraisals. In particular, tilt systems identified by Glazer in which both in-phase and anti-phase tilts have the same magnitude are inconsistent with Landau's theory of second-order phase transitions (Landau & Lifshitz 1996), which only permits a single point in reciprocal space to become

critical. Hence, the equality in magnitude of symmetry-independent modes can only occur accidentally, and cannot be representative of a stable phase over a range of pressure–temperature space. As a result, the number of tilt systems is less than the twenty-three originally proposed by Glazer. Furthermore, experimental work on the compound $CaFe_2TiO_6$ showed the space group assigned to the tilt system $a^+a^+c^-$, *Pmmn*, to be in error, and the correct space-group should in fact be $P4_2/nmc$ (Leinenweber & Parise 1995).

In recent years, the problem of rigorously determining the correct space-groups and lattice metrics for the subgroups of the aristotype phase, subjected to a wide variety of structural distortions and schemes of chemical ordering, has been carried out using the group theory by Howard and co-workers (Howard & Stokes 1998, 2002, 2005, Howard *et al.* 2002, 2003, Howard & Zhang 2004a, 2004b, Stokes *et al.* 2002). Using the software ISOTROPY (www.physics.byu.edu/~stokesh/isotropy.html), Howard & Stokes (1998, 2002) determined the isotropy subgroups of the aristotype phase for the representation given by the direct sum $M_3^+ \oplus R_4^+$, *i.e.*, those subgroups consistent with in-phase and anti-phase tilting of the BX_6 octahedra. Of the twenty-five distinct isotropy subgroups found using ISOTROPY, only fourteen permit simple rotations of octahedra around <100>, and hence this set forms the allowed subgroups for the zone-boundary-tilted centrosymmetric perovskite hettotype phases. Howard & Stokes tabulated the fourteen space-groups and, using a tree diagram, showed how the tilt systems related to one another through hypothetical phase-transitions, in which the nature of the transition was identified as either discontinuous or potentially continuous. In finalizing this number of space groups, Howard & Stokes (1998) verified the experimental results of Leinenweber & Parise (1995), that is the space group associated with the tilt system $a^+a^+c^-$ is $P4_2/nmc$ and not *Pmmn*.

Although group theory has permitted a rigorous classification of perovskite and elpasolite subgroups for the first time, the parameterization of the crystal structures of these phases, in contrast, has remained at best semi-empirical; fairly recent examples of parameterization are provided in the work of Ranløv (1995) and Thomas (1998). Ranløv (1995) applied principal component analysis to the temperature dependence of the crystal structure of $TbAl_{0.95}Mg_{0.05}O_{3-\delta}$, and found, probably unsurprisingly, that the TbO_{12} polyhedron becomes more regular with increasing temperature as the magnitude of the tilt angles of the octahedra lessens. Thomas (1998) has described a geometrically complex parameterization for tetragonal, rhombohedral and orthorhombic perovskites using the ratio of the polyhedron volumes of the A and B sites and eight distances and angles defined in projection. However, this method relies totally on an empirical analysis of *known* crystal structures, and, as Mitchell (2002) has noted in his monograph, the method has not become widely used by workers in the

field. It is therefore somewhat surprising to note that the first precise parameterization of perovskite hettotypes in fact predates the work of Glazer (1972). In a paper essentially about the dynamics of zone-boundary phase transitions in perovskites, Cochran & Zia (1968) carried out a decomposition of the atomic displacements for two oxide perovskites ($LaAlO_3$ and $CaTiO_3$) in terms of the weights of frozen modes of a hypothetical aristotype phase. This methodology was not immediately followed up by the crystallographic community at the time, and over thirty years later, Darlington (2002a, 2002b) carried out a similar detailed analysis for nine hettotype phases of perovskite and elpasolite. Knight *et al.* (2005a, 2005b) analyzed high-pressure results on $SrCeO_3$ and low-temperature results on $KCaF_3$ using the lattice-dynamical analysis of Cochran & Zia (1968), but unfortunately they did not relate the changes in the mode magnitudes to the changes in the crystal structure. Mitchell *et al.* (2007) have presented mode-displacement amplitudes for $NaMgF_3$ at 3.6 and 300 K. An extremely detailed study of the octahedron tilt modes in the perovskite-related compounds ABX_4 and A_2BX_4 has been made by Swainson (2005); in that case, displacements have been analyzed in terms of the primitive tetragonal Brillouin zone. However, in a recent study of the thermoelastic properties of the protonic conducting perovskite $SrCe_{0.95}Yb_{0.05}O_\xi$ ($\xi \approx 3$), Knight *et al.* (in prep.) have discussed the temperature dependence of the crystal structure purely in terms of the magnitudes of the condensed modes of a hypothetical aristotype phase.

Methodology

Determination of the symmetry-adapted basis-vectors

The decomposition of the fractional coordinates of perovskite-structured materials in terms of the appropriate set of symmetry-adapted basis-vectors for each of the fourteen space-groups consistent with simple tilting of the octahedra has been determined by applying representation analysis to the aristotype phase at key points in reciprocal space. The methodology for determining the symmetry of lattice vibrations in crystals has been described in detail by Montgomery (1969), but the method briefly described below is derived from the study of the structural and magnetic phase-transition in $SrMnO_3$ by Daoud-Aladine *et al.* (2007).

The atomic positions in the lower-symmetry phase are written

$$\mathbf{r}_{ni} = \mathbf{r}_i^0 + \mathbf{u}_{ni}$$

for atoms in the unit cell indexed by $\mathbf{R}_n$ that occupy position $\mathbf{r}_i^0$ in the aristotype phase, and which are now displaced by vectors $\mathbf{u}_{ni}$. The displacement vectors are decomposed with the Fourier sum

$$\mathbf{u}_{ni} = \sum_{\mathbf{k}} (\mathbf{u}_{\mathbf{k}}^i e^{2\pi i \mathbf{k} \cdot \mathbf{R}_n} + \mathbf{u}_{\mathbf{k}}^{i*} e^{-2\pi i \mathbf{k} \cdot \mathbf{R}_n})$$

where $\mathbf{k}$ is the wave-vector characterizing the way the translational symmetry is broken on entering the lower-symmetry phase. In most simple perovskite hettotypes, the unit-cell dimensions double at most in the lower-symmetry phases (bipartite hettotypes), and as a result, only the wave-vectors $\mathbf{k} = (0\ 0\ ½)$, $(½\ ½\ 0)$ and $(½\ ½\ ½)$ have to be considered in calculating the symmetry-adapted basis-vectors. For each wave-vector in turn, the symmetry relationships between the vectors $\mathbf{u}_{ni}$ of the same crystallographic orbit are obtained for each *irrep* Γ_v using the projection operator

$$\hat{P}^v = \left\{ \sum_{g=G_k} D_{\lambda\mu}^{*v}(g)\hat{g} \right\}$$

where the sum is over the symmetry elements of the little group that transforms $\mathbf{k}$ into an equivalent wave-vector and $D_{\lambda\mu}^{*v}(g)$ are the elements of the matrix representation of g for the *irrep v*.

Cowley (1964) was the first to carry out this analysis for the aristotype phase of perovskite calculating the *sabvs* along the Δ $(0\ 0\ \xi)$, Σ $(\xi\ \xi\ 0)$ and Λ $(\xi\ \xi\ \xi)$ lines of the cubic Brillouin zone (Koster 1957), with the results being tabulated as an appendix to his paper. Table 1 shows the results of Cowley for the *sabvs* for the aristotype phase of perovskite calculated at the wave-vectors $\mathbf{k} = (0\ 0\ ½)$, $(½\ ½\ 0)$ and $(½\ ½\ ½)$. In the Table, the *irreps* are labeled according to the notation of Miller and Love (Bradley & Cracknell 1972); for completeness, Cowley's original notation for the *irreps* is given in parentheses. The fractional coordinates of the three anions are differentiated following Cowley's labeling; X_I $(0\ 0\ ½)$, X_{II} $(0\ ½\ 0)$ and X_{III} $(½\ 0\ 0)$. The *sabvs* reproduced in Table 1 have been independently verified by using two computer programs, Isotropy and Basireps (http://www.ill.fr/dif/Soft/fp/php/programsfa7c.html?pagina=GBasireps). Most of the tabulated basis-vectors shown in Table 1 are not found as frozen displacements within the perovskite hettotype phases, and to parameterize the crystal structure of any hettotype phase, all that is necessary is to identify the set that is potentially present for any particular space-group.

To decompose the fractional coordinates for each of the perovskite subgroups, the following assumptions are made:

1) The atomic displacements found in a centrosymmetric, bipartite hettotype can be described in terms of the magnitudes of a set of orthogonal, symmetry-adapted basis-vectors of the aristotype phase. The only basis-vectors that can condense out to produce the hettotype phase have wave-vectors at the R, M and X

points of the cubic Brillouin zone: these are $\frac{1}{2}$ [$\mathbf{a}^*$ + $\mathbf{b}^*$ + $\mathbf{c}^*$], $\frac{1}{2}$ [$\mathbf{a}^*$ + $\mathbf{b}^*$] (or symmetry-related points) and $\frac{1}{2}$ [$\mathbf{c}^*$] (or symmetry-related points), respectively.

2) Each term in the Landau expansion of the excess free energy associated with a phase transition must be invariant with respect to all symmetry operations of the aristotype phase, *i.e.*, the wave-vectors of the

TABLE 1. SYMMETRY-ADAPTED BASIS-VECTORS FOR THE ARISTOTYPE PHASE OF PEROVSKITE CALCULATED AT THE X POINT, $\mathbf{k}$ = (0 0 $\frac{1}{2}$), THE M POINT, $\mathbf{k}$ = ($\frac{1}{2}$ $\frac{1}{2}$ 0), AND THE R POINT, $\mathbf{k}$ = ($\frac{1}{2}$ $\frac{1}{2}$ $\frac{1}{2}$) OF THE CUBIC BRILLOUIN ZONE*

$\mathbf{k}$ = (0 0 $\frac{1}{2}$)			
Irreducible representation		Displacements	
X_3^- (M1)	B(z)	$X_{II}(z) = X_{III}(z)$	
X_1^+ (M2')	A(z)	$X_I(z)$	
X_4^- (M3)	$X_{II}(z) = -X_{III}(z)$		
X_5^- (M5)	B(x)	$X_{II}(x)$	$X_{III}(x)$
X_5^- (M5)	B(y)	$X_{II}(y)$	$X_{III}(y)$
X_5^+ (M5')	A(x)	$X_I(x)$	
X_5^+ (M5')	A(y)	$X_I(y)$	

$\mathbf{k}$ = ($\frac{1}{2}$ $\frac{1}{2}$ 0)			
Irreducible representation		Displacements	
M_4^+ (M1)	$X_{II}(x) = X_{III}(y)$		
M_2^+ (M2)	$X_{III}(x) = -X_{II}(y)$		
M_3^+ (M3)	$X_{II}(x) = -X_{III}(y)$		
M_1^+ (M4)	$X_{III}(x) = X_{II}(y)$		
M_2^- (M2')	A(z)		
M_3^- (M3')	B(z)	$X_I(z)$	
M_5^+ (M5)	$X_{II}(z)$		
M_5^+ (M5)	$X_{III}(z)$		
M_5^- (M5')	B(x)	A(y)	$X_I(x)$
M_5^- (M5')	B(y)	A(x)	$X_I(y)$

$\mathbf{k}$ = ($\frac{1}{2}$ $\frac{1}{2}$ $\frac{1}{2}$)			
Irreducible representation		Displacements	
R_1^+ (Γ2')	$X_I(z) = X_{II}(y) = X_{III}(x)$		
R_3^+ (Γ12')	$X_I(z) = X_{II}(y) = -\frac{1}{2} X_{III}(x)$		
R_3^+ (Γ12')	$X_I(z) = -X_{II}(y)$		
R_4^+ (Γ25)	$X_I(y) = -X_{II}(z)$		
R_4^+ (Γ25)	$X_I(x) = -X_{III}(z)$		
R_4^+ (Γ25)	$X_{II}(x) = -X_{III}(y)$		
R_4^- (Γ25')	B(x)		
R_4^- (Γ25')	B(y)		
R_4^- (Γ25')	B(z)		
R_5^+ (Γ15')	A(x)	$X_I(y) = X_{II}(z)$	
R_5^+ (Γ15')	A(y)	$X_I(x) = X_{III}(z)$	
R_5^+ (Γ15')	A(z)	$X_{II}(x) = X_{III}(y)$	

* The irreducible representations use the notation of Miller and Love (Bradley & Cracknell 1972), with those of Cowley (1964) given in parentheses.

order parameters within that term must sum to zero or a reciprocal lattice vector. From assumption 1, it is clear that the sum of the three quoted wave-vectors is a reciprocal lattice vector of the aristotype, and hence displacements with wave-vector equal to $\frac{1}{2}$ [$\mathbf{c}^*$] (or symmetry-related points) can only occur where both in-phase and anti-phase tilts of the octahedra are present in the structure.

3) The number of independent condensed basis-vectors equals the number of degrees of freedom of the crystal structure in the particular space-group.

4) Where it is necessary for two basis-vectors to have equal magnitudes of displacement, they are required to have the same irreducible representation, but may have symmetry-related wave-vectors.

Hence, to determine the effect of any basis-vector displacement, a supercell of size 2 × 2 × 2 of the parent aristotype is required. Figure 1 illustrates eight such unit cells viewed down [001] with the *B* site placed at the origin of the unit cell. The anion X_I at (0 0 $\frac{1}{2}$) is cross-hatched, the anions X_{II} at (0 $\frac{1}{2}$ 0) and X_{III} at ($\frac{1}{2}$ 0 0) are both white, whereas the *A* site at ($\frac{1}{2}$ $\frac{1}{2}$ $\frac{1}{2}$) is black. The right-hand set of four unit cells sits on top of the left-hand set, giving rise to the complete 2 × 2 × 2 supercell. For some space groups, the unit-cell basis-vectors are related to the aristotype through the transformations 1$\bar{1}$0/110/001 or 1$\bar{1}$0/110/002, and the associated unit-cell is shown in the Figure with dashed lines. The wave-vector associated with the *irrep* indicates the direction(s) of unit-cell doubling, and a displacement vector is required to reverse in the neighboring unit-cell if the unit-cell doubles in that particular direction.

A-site displacements

The *A*-site displacements are only found in perovskite hettotypes that exhibit anti-phase tilting alone or those that permit both in-phase and anti-phase tilting; in either case the number of independent *A* sites is usually small. By contrast, hettotypes consistent with pure in-phase tilting show no atomic displacements but are generally characterized by the large number of symmetry-independent *A* sites.

Consider the *A* site in a hettotype with space group *Pbnm*, lattice basis-vectors 1$\bar{1}$0/110/002 and Glazer symbol a⁻a⁻c⁺. For the four sites labeled 1, 2, 5, 6 in Figure 1, which are taken to be related by *Pbnm* space-group symmetry, the fractional coordinates are given by: $\frac{1}{2} - u, v, \frac{1}{4}$; $u, \frac{1}{2} + v, \frac{1}{4}$; $\frac{1}{2} + u, -v, \frac{3}{4}$; and $-u, \frac{1}{2} - v, \frac{3}{4}$, where u and v are generally small. If a component of a displacement vector $\Delta\mathbf{r}$ has R point character, then this component is identical in magnitude and direction for sites 1, 4, 6, 7, and in the opposite direction, but with equal magnitude, for sites 2, 3, 5, 8. For a component with M point character and wave-vector $\frac{1}{2}$ [$\mathbf{a}^*$ + $\mathbf{b}^*$], the magnitude of the displacement at sites 1, 4, 5, 8, is equal and opposite to that for the sites 2, 3, 6, 7, whereas for

the X point with wave-vector ½ [$\mathbf{c}$*], the magnitude of the displacement at sites 1, 2, 3, 4 is equal and opposite to that for the sites 5, 6, 7, 8. The displacement pattern for the fractional coordinate displacement u can clearly be seen to be consistent with the R point, whereas that for v is consistent with the X point. From the data shown in Table 1, only one *irrep* is associated with the *A* site at the R point, namely R_5^+ with *sabvs* A(x) and A(y), but these displacements are associated with the x and y directions of a cubic cell and not the x direction of an orthorhombic cell. Allowing these two displacements to have equal magnitude, with the correct relative phase, the vector sum will be in the x direction of an orthorhombic cell, and with the required R point character. Note that this result clearly ignores the second-order effect of the non-orthogonality of pseudocubic subcell associated with the orthorhombic unit-cell; taking the unit cell of $CaTiO_3$ at room temperature as a typical example, the deviation of the shear angle from 90° is only of the order of 0.6°. Using a similar argument, the displacements in the y direction of an orthorhombic cell can be shown to arise from two equal-magnitude *sabvs* A(x) and A(y) with *irrep* X_5^+. The displacement patterns associated with these two pairs of *irreps* are illustrated in Figure 2.

Writing the magnitude of the *sabv* A(x) with *irrep* R_5^+ as d_1, and that with *sabv* A(x) with *irrep* X_5^+ as d_2, the fractional coordinates of the *A* site in terms of the

sabvs and the orthorhombic lattice constants a, b, c are therefore

$$\frac{\sqrt{2}d_1}{a}, \frac{1}{2} + \frac{\sqrt{2}d_2}{b}, \frac{1}{4}.$$

The same methodology can be applied to all the space groups determined by Howard & Stokes (1998, 2002) that exhibit *A*-site displacements, with only one particular space-group requiring additional detailed comments (Darlington 2002a, supplementary material). In space group $P4_2/nmc$, the *A* site splits into three orbits with Wyckoff positions 2a, 2b and 4d, which correspond to the labeled sites in Figure 1, (2, 7), (3, 6) and (1, 4, 5, 8), respectively. Wyckoff positions 2a and 2b have fixed coordinates, whereas 4d (¼ ¼ ¼ + w) allows for displacements along [0 0 1]. To produce this pattern of displacements, it is necessary to have *sabvs* that cancel on the first two Wyckoff sites (2a, 2b) and reinforce on the third site (4d). As the space group allows for both in-phase and anti-phase tilting, displacements with X point character are therefore permitted. Following on from assumption 4, and transforming the results given in Table 1, it can be seen that this complex pattern of displacement can be replicated by two *sabvs* A(z) with equal magnitude but opposite directions of displacement and symmetry-related *irreps* [½ 0 0] X_5^+ and [0 ½ 0] X_5^+.
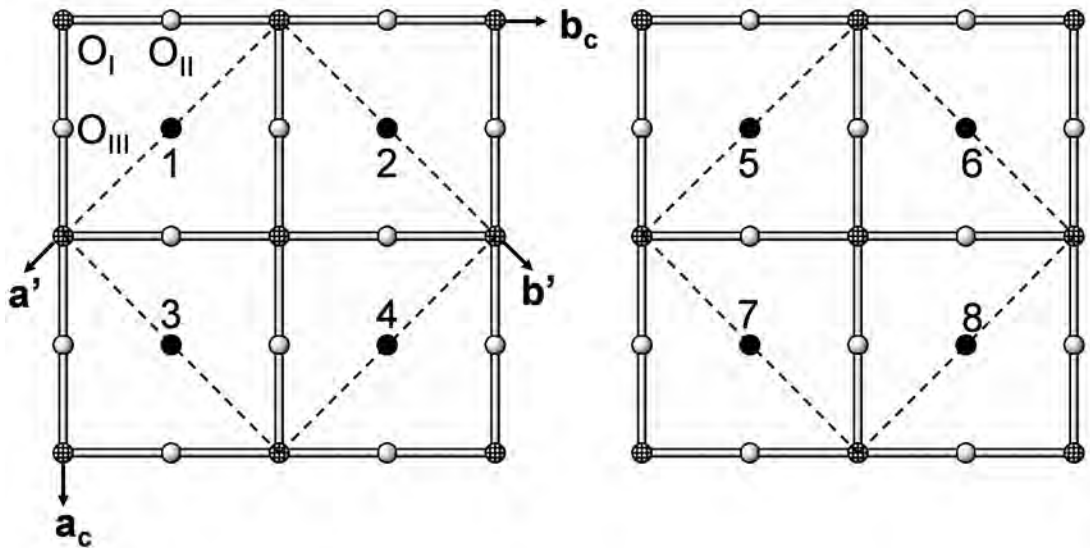

FIG. 1.   A 2 × 2 × 2 supercell of perovskite, with the right-hand set of four subcells sitting on top of the left-hand set of four subcells. The conventional unit-cell of perovskite is designated by vectors subscripted c, the rotated unit-cell of perovskite is shown by dotted lines and vectors superscripted by primes. The three anions are differentiated using the labeling of Cowley (1964), whereas the *A*-site cations are numbered one to eight to aid discussion of the displacement patterns for three symmetry-adapted basis-vectors with irreducible representations at the R point, M point and X point of the cubic Brillouin zone.
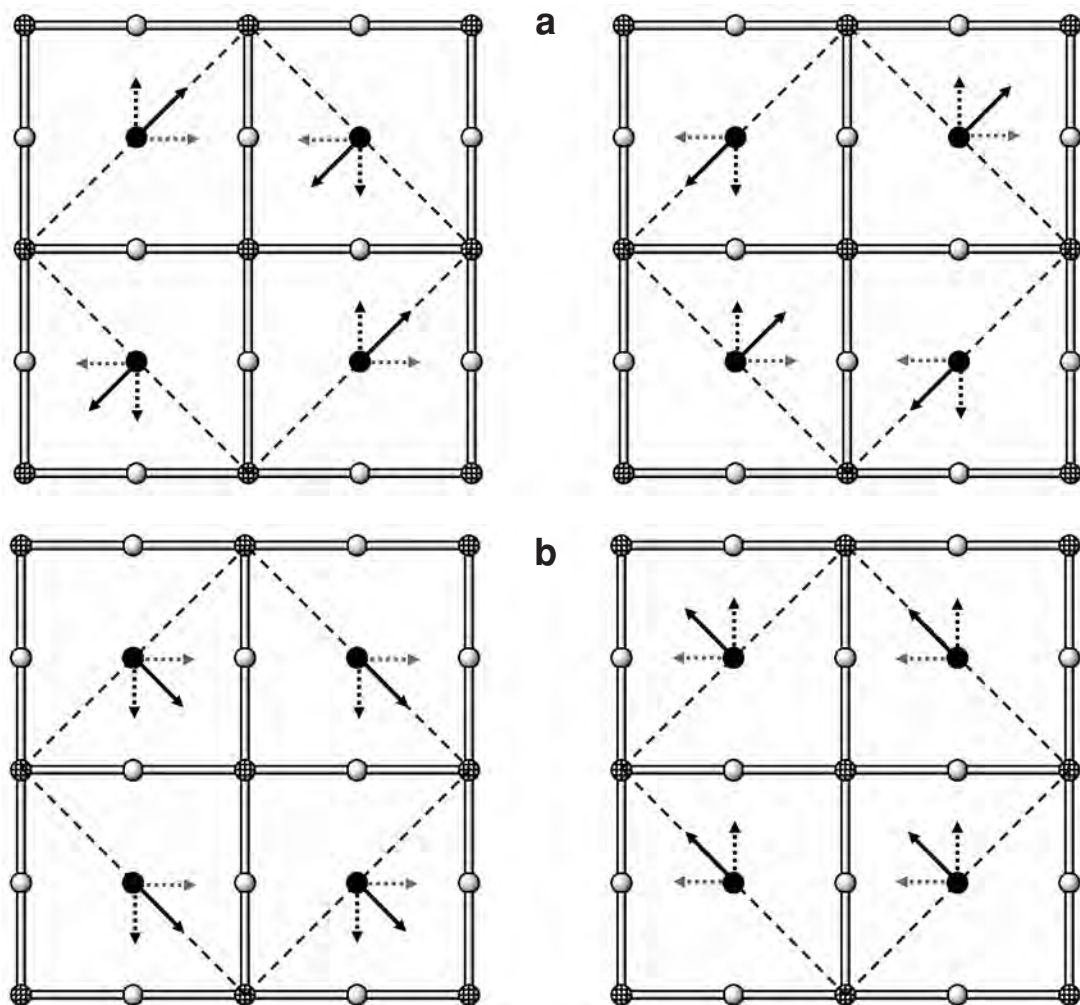
FIG. 2. a) Displacement patterns of the *A* site associated with the symmetry-adapted basis-vectors at the R point. Black dotted arrow: irreducible representation R_5^+ with symmetry-adapted basis-vector A(x), grey dotted arrow: the same irreducible representation with symmetry-adapted basis-vector A(y). The resultant vector in the orthorhombic x direction is shown as the full black arrow. b) Displacement patterns of the *A* site associated with the symmetry-adapted basis-vectors at the X point. Black dotted arrow: irreducible representation X_5^+ with symmetry-adapted basis-vector A(x), grey dotted arrow: irreducible representation X_5^+ with symmetry-adapted basis-vector A(y). The resultant vector in the orthorhombic y direction is shown as the full black arrow.

Anion displacements

For all the centrosymmetric space-groups of perovskite consistent with simple tilting of octahedra, the number of independent anion positions either leaves the Cowley anion classes undifferentiated (*e.g.*, in space group $Im\bar{3}$, there is a unique anion position), partially differentiated (*e.g.*, in space group $I2_1/b\,1\,1$, one anion site is associated with X_I, whereas the second is asso-

ciated with X_{II} and X_{III}) or unmixed (*e.g.*, each of the three independent anion positions in space group $F\bar{1}$ is uniquely associated with either X_I, X_{II}, or X_{III}).

If the anion displacements in the space group *Pbnm* are taken as an example, the fractional coordinates for the two anion sites O1 and O2 are $u1$, $v1$, ¼ and ¼ + $u2$, ¼ + $v2$, $w2$, respectively, where O1 is associated with X_I, O2 is associated with both X_{II} and X_{III}, and the displacement magnitudes $u1$, $v1$, $u2$, $v2$ and $w2$ are

generally small. The Glazer symbol for this space group is $a^-a^-c^+$, and writing d_3 for the magnitude of the *sabv* associated with the anti-phase tilt [*irrep* R_4^+, either *sabv* $X_I(x) = -X_{III}(z)$, or *sabv* $X_I(y) = -X_{II}(z)$], and d_4 for the corresponding magnitude of the *sabv* for the in-phase tilt [(*irrep* M_3^+, *sabv* $X_{II}(x) = -X_{III}(y)$], the fractional coordinates become:

$$\frac{\sqrt{2}d_3}{a}, 0, \frac{1}{4}$$

$$\frac{1}{4} - \frac{d_4}{\sqrt{2}a}, \frac{1}{4} + \frac{d_4}{\sqrt{2}b}, -\frac{d_3}{c}.$$

For regular tilted octahedra, the following ratios therefore apply:

$$\frac{u1}{w2} = \frac{-\sqrt{2}c}{a} \approx -2$$

$$\frac{u2}{v2} = \frac{-b}{a} \approx -1$$

i.e., the individual atomic displacements are not linearly independent in this simple model case. For CaTiO$_3$ at ambient temperature (see the RESULTS section for more details), $u1/w2$ is equal to -1.933 and $u2/v2$ is equal to -1.013, indicating that there is only a modest distortion of the TiO$_6$ octahedron from ideality. This is in contrast to the crystal structure of KCaF$_3$ at 4.2 K, where $u1/w2$ is equal to -1.874 and $u2/v2$ is equal to -1.033, both values indicating a more significant deformation of the CaF$_6$ octahedron in this case (Knight *et al.* 2005b).

To break the linear dependence of $u1$ with $w2$, it is necessary to find a *sabv* that permits displacements in the orthorhombic x direction for O1 and the z direction for O2. Noting that O1, like the A site, sits on a mirror plane, the same symmetry arguments that applied for the A site will apply yet again. Therefore, the required *sabv* has to have R point character. Examination of Table 1 shows that this can be satisfied by two equal magnitude *sabvs*, $X_I(x) = X_{III}(z)$ and $X_I(y) = X_{II}(z)$ with *irrep* R_5^+. Further consideration of the symmetry of the O1 site and Table 1 shows that $v1$ is associated with two equal-magnitude *sabvs*, $X_I(x)$ and $X_I(y)$, with *irrep* X_5^+. Finally, to break the linear dependence of $u2$ with $v2$, a *sabv* is required that differentiates $X_{III}(x)$ from $X_{II}(y)$. To be consistent with the in-phase tilt displacement, this *sabv* has to have M point character. Inspection of Table 1 shows this mode to have *irrep* M_2^+ with *sabv* $X_{III}(x) = -X_{II}(y)$.

Gathering these results together, the fractional coordinates for a perovskite in space group *Pbnm* written in terms of symmetry-adapted basis-vectors is therefore

A $\frac{\sqrt{2}d_1}{a}, \frac{1}{2} + \frac{\sqrt{2}d_2}{b}, \frac{1}{4}$

B $0, 0, 0$

O1 $\frac{\sqrt{2}(d_3 - d_7)}{a}, \frac{\sqrt{2}d_5}{b}, \frac{1}{4}$

O2 $\frac{1}{4} - \frac{(d_4 - d_6)}{a\sqrt{2}}, \frac{1}{4} + \frac{(d_4 + d_6)}{b\sqrt{2}}, \frac{-(d_3 + d_7)}{c}$

where d_5 is the magnitude of the *sabv* $X_I(x)$ with *irrep* X_5^+, d_6 is the magnitude of the *sabv* $X_{III}(x) = -X_{II}(y)$ with *irrep* M_2^+, and d_7 is the magnitude of the *sabv* $X_I(x)$ with *irrep* R_5^+.

RESULTS

An identical analysis to that outlined above for space group *Pbnm* can be carried out for all of the thirteen remaining space-groups. The analysis presented in the previous section shows that the displacements of the fractional coordinates from the ideal positions that they would occupy in the aristotype phase can be written as a linear combination of the magnitudes of a set of symmetry-adapted basis-vectors of the aristotype phase. Writing **d** as the column vector of the *sabv* magnitudes and **r** as the column vector related to the physical displacements for specific atoms, then **r** = **Md**, and hence **d** = **M^{-1}r**. Any centrosymmetric, tilted perovskite structure can therefore be simply decomposed (parameterized) in terms of the magnitudes of the appropriate symmetry-adapted basis-vectors, the orthogonality of the basis-vectors ensuring that the solution is unique.

The fractional coordinates, lattice basis, symmetry-adapted basis-vectors, displacement vectors, the non-zero elements of matrix **M,** and its inverse, are listed in Tables 2a–e, 3a–f and 4a–d for the fourteen centro-symmetric perovskite hettotype space-groups consistent with zone-boundary tilting. Tables 2a–e relate to the pure in-phase tilted hettotypes, and includes the aristotype for completeness, Tables 3a–f pertain to the pure anti-phase tilted hettotypes, whereas the space groups consistent with both in- and anti-phase tilting are dealt with in Tables 4a–d. To avoid potential confusion with the matrix elements M_{jk} of **M**, in the Tables, the non-zero elements of **M^{-1}** are labeled Mi_{lm}.

The space-group settings have been chosen such that the interaxial angles are as close to 90° as possible; hence for the tilt system $a^-a^-a^-$, $F\bar{3}2/n$ is used in preference to $R\bar{3}c$ in either the primitive rhombohedral or hexagonal settings; for $a^-b^-c^-$, $F\bar{1}$ is used over $P\bar{1}$ or $I\bar{1}$ for the same reason. Where at all possible, the B site has been placed at the origin of the unit cell. Statistical analysis of the frequency of occurrence of the tilt systems of octahedra in perovskites (Lufaso & Woodward 2001) has shown that ~50% exhibit the tilt system $a^-a^-c^+$ in

space group *Pbnm* or some alternative setting of space group No. 62. Numerous structural phase-transition sequences starting from this tilt system have been characterized, and to enable ease of comparison of *sabvs* from lower- or higher-symmetry space-groups that could be related by a continuous phase-transition from *Pbnm*, the lattice basis $1\bar{1}0/110/002$ for these subgroups and supergroups has been chosen. This inevitably leads to non-standard space-group settings, and where these are particularly unusual, the group generators are also included in Table 3.

DISCUSSION AND EXAMPLES OF APPLICATION

Taking the room-temperature crystal structure of $CaTiO_3$ in space group *Pbnm* as an illustrative example, and using the results from Table 4b, the relationship between the magnitudes of the *sabvs* and the atomic displacements is given by:
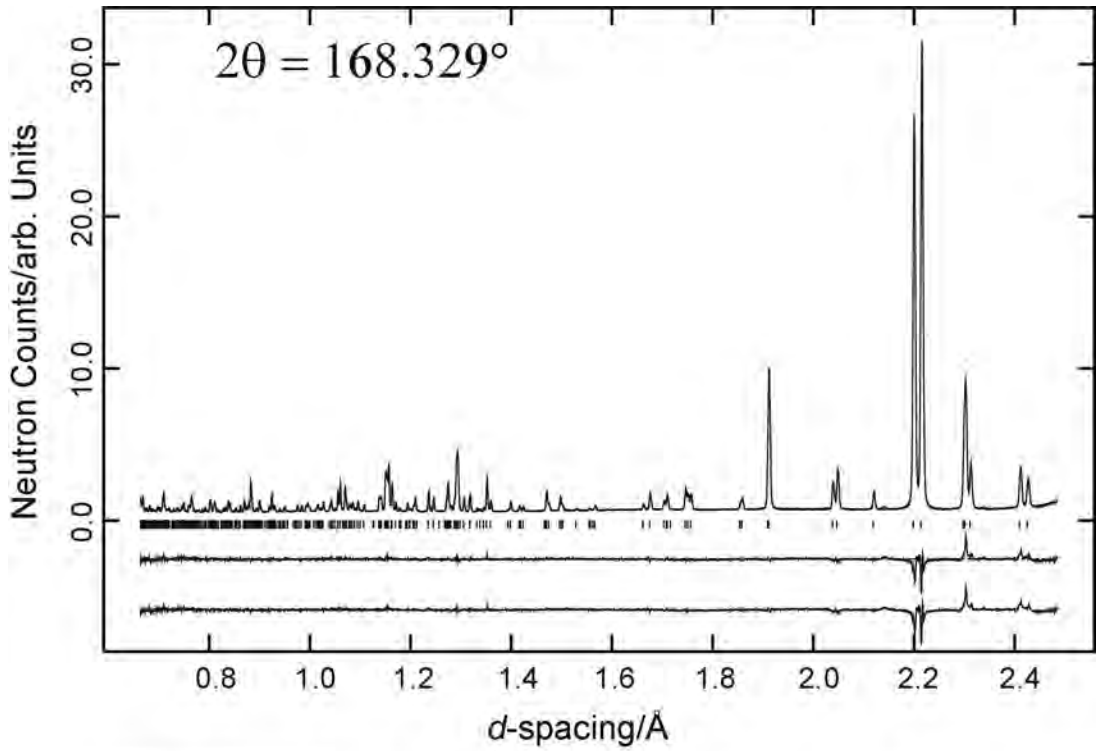
$$\begin{pmatrix} 1 & 0 & 0 & 0 & 0 & 0 & 0 \\ 0 & 1 & 0 & 0 & 0 & 0 & 0 \\ 0 & 0 & 1 & 0 & 0 & 0 & -1 \\ 0 & 0 & 0 & 0 & 1 & 0 & 0 \\ 0 & 0 & 0 & -1 & 0 & 1 & 0 \\ 0 & 0 & 0 & 1 & 0 & 1 & 0 \\ 0 & 0 & -1 & 0 & 0 & 0 & -1 \end{pmatrix} \begin{pmatrix} d_1 \\ d_2 \\ d_3 \\ d_4 \\ d_5 \\ d_6 \\ d_7 \end{pmatrix} = \begin{pmatrix} au/\sqrt{2} \\ bv/\sqrt{2} \\ au1/\sqrt{2} \\ bv1/\sqrt{2} \\ \sqrt{2}au2 \\ \sqrt{2}bv2 \\ cw2 \end{pmatrix}$$

TABLES 2a–e. DECOMPOSITION OF THE ARISTOTYPE PHASE AND ISOTROPY SUBGROUPS
CONSISTENT WITH IN-PHASE TILTING ALONE

2a

Space group	M_3^+	R_4^+	Tilts	Lattice vectors
$Pm\bar{3}m$ (No. 221)	(0,0,0)	(0,0,0)	$a^0a^0a^0$	100 / 010 / 001

A	B	Cowley label	X
1b, ½,½,½	1a, 0,0,0	O_I, O_{II}, O_{III}	3d, ½,0,0

2b

Space group	M_3^+	R_4^+	Tilts	Lattice vectors
P4/mbm (No. 127)	(0,0,c)	(0,0,0)	$a^0a^0c^+$	110 / 1$\bar{1}$0 / 001

A	B	Cowley label	X
2c, 0,½, ½	2a, 0,0,0	O_I	2b, 0,0,½
		O_{II}, O_{III}	4g, ¼−u2, ¼+u2,0

Irreducible representation	Label	Displacement
[½½0] M $_3^+$	d_1	$O_{II}(x) = -O_{III}(y)$

$d_1 = \sqrt{2}au2$

2c

Space group	M_3^+	R_4^+	Tilts	Lattice vectors
I4/mmm (No. 139)	(a,a,0)	(0,0,0)	$a^+a^+c^0$	200 / 020 / 002

A	B	Cowley label	X
2a, 0,0,0	8f, ¼,¼,¼	O_I	8h, ¼+u1,¼+u1,0
2b, 0,0,½		O_{II}, O_{III}	16n, 0,¼+v2,¼+w2
4c, ½,0,0			

Irreducible representation	Label	Displacement
[0½½] M $_3^+$	d_1	$O_{II}(z) = -O_I(y)$
[½0½] M $_3^+$	d_1	$O_{III}(z) = -O_I(x)$
[½½0] M $_4^+$	d_2	$O_{II}(x) = O_{III}(y)$
[0½½] M $_4^+$	d_3	$O_{II}(z) = O_I(y)$
[½0½] M $_4^+$	d_3	$O_{III}(z) = O_I(x)$

$r_1 = au1, r_2 = av2, r_3 = cw2$
$M_{11} = M_{13} = M_{22} = M_{33} = 1; M_{31} = -1$
$Mi_{22} = 1; Mi_{11} = Mi_{31} = Mi_{33} = 1/2; Mi_{13} = -1/2$

2d

Space group	M_3^+	R_4^+	Tilts	Lattice vectors
$Im\bar{3}$ (No. 204)	(a,a,a)	(0,0,0)	$a^+a^+a^+$	200 / 020 / 002

A	B	Cowley label	X
2a, 0,0,0	8c, ¼,¼,¼	O_I, O_{II}, O_{III}	24g, ¼+u1,¼+v1,0
6b, 0,½,½			

Irreducible representation	Label	Displacement
[½½0] M $_3^+$	d_1	$O_{II}(x) = -O_{III}(y)$
[0½½] M $_3^+$	d_1	$O_I(z) = -O_I(y)$
[½0½] M $_3^+$	d_1	$O_{III}(z) = -O_I(x)$
[½½0] M $_4^+$	d_2	$O_{II}(x) = O_{III}(y)$
[0½½] M $_4^+$	d_2	$O_I(z) = O_I(y)$
[½0½] M $_4^+$	d_2	$O_{III}(z) = O_I(x)$

$r_1 = au1, r_2 = av1$
$M_{11} = M_{12} = M_{22} = 1; M_{12} = -1$
$Mi_{11} = Mi_{21} = Mi_{22} = 1/2; Mi_{12} = -1/2$

2e

Space group	M_3^+	R_4^+	Tilts	Lattice vectors
Immm (No. 71)	(a,b,c)	(0,0,0)	$a^+b^+c^+$	200 / 020 / 002

A	B	Cowley label	X
2a, 0,0,0	8k, ¼,¼,¼	O_I	8n, ¼+u1,¼+v1,0
2b, 0,½,½		O_{II}	8m, ¼+u2,0,¼+w2
2c, ½,½,0		O_{III}	8l, 0,¼+v3,¼+w3
2d, ½,0,½			

Irreducible representation	Label	Displacement
[0½½] M $_3^+$	d_1	$O_{II}(z) = -O_I(y)$
[½0½] M $_3^+$	d_2	$O_{II}(z) = -O_I(x)$
[½½0] M $_3^+$	d_3	$O_{II}(x) = -O_{III}(y)$
[0½½] M $_4^+$	d_4	$O_{II}(z) = O_I(y)$
[½0½] M $_4^+$	d_5	$O_{III}(z) = O_I(x)$
[½½0] M $_4^+$	d_6	$O_{II}(x) = O_{III}(y)$

$r_1 = au1, r_2 = bv1, r_3 = au2, r_4 = cw2, r_5 = bv3, r_6 = cw3$
$M_{12} = M_{15} = M_{24} = M_{36} = M_{41} = M_{44} = M_{53} = M_{66} = M_{65} = 1; M_{21} = M_{33} = M_{62} = -1$
$Mi_{14} = M_{21} = Mi_{35} = Mi_{42} = Mi_{44} = Mi_{51} = Mi_{56} = Mi_{63} = Mi_{65} = 1/2; Mi_{17} = Mi_{26} = Mi_{33} = -1/2$

TABLES 3a–f. DECOMPOSITION OF THE ISOTROPY SUBGROUPS CONSISTENT WITH ANTI-PHASE TILTING ALONE

3a

Space group	M_3^+	R_4^+	Tilts	Lattice vectors
$I4/mcm$ (No. 140)	(0,0,0)	(0,0,c)	$a^0a^0c^-$	110 / 1$\overline{1}$0 / 002

A	B		Cowley label	X
4b, 0,½,¼	4c, 0,0,0		O_I	4a, 0,0,¼
			O_{II}, O_{III}	8h, ¼–u2,¼+u2,0

Irreducible representation	Label	Displacement
[½½½] R_4^+	d_1	$O_{II}(x) = -O_{III}(y)$

$d_1 = \sqrt{2}au2$

3b

Space group	M_3^+	R_4^+	Tilts	Lattice vectors
$Ibnn$ (No. 74)	(0,0,0)	(a,a,0)	$a^-a^-c^0$	110 / 1$\overline{1}$0 / 002

Group generators: ½ + x, ½ + y, ½ + z; x, y, ½ – z; x, –y, z; –x, –y, –z

A	B		Cowley label	X
4e, ½+u,0,¼	4b, 0,0,0		O_I	4e, u1,0,¼
			O_{II}, O_{III}	8f, ¼,¼,w2

Irreducible representation	Label	Displacement
[½½½] R_5^+	d_1	A(x)
[½½½] R_5^+	d_1	A(y)
[½½½] R_4^+	d_2	$O_I(y) = -O_{II}(z)$
[½½½] R_4^+	d_2	$O_I(x) = -O_{III}(z)$
[½½½] R_4^+	d_3	$O_I(y) = O_{II}(z)$
[½½½] R_5^+	d_3	$O_I(x) = O_{III}(z)$

$r_1 = au/\sqrt{2}$, $r_2 = au1/\sqrt{2}$, $r_3 = cw2$
$M_{11} = M_{22} = M_{23} = M_{33} = 1$; $M_{22} = -1$
$Mi_{11} = 1$; $Mi_{22} = Mi_{32} = Mi_{33} = 1/2$; $Mi_{23} = -1/2$

3c

Space group	M_3^+	R_4^+	Tilts	Lattice vectors
$F\overline{3}2/n$ (No. 167)	(0,0,0)	(a,a,a)	a a a	200 / 020 / 002

Group generators: ½ + x, ½ + y, z; z, x, y; ½ – y, ½ – x, ½ – z; –x, –y, –z

A	B	Cowley label	X
8a, ¼,¼,¼	8b, 0,0,0	O_I, O_{II}, O_{III}	24e, –u1,u1,¼

Irreducible representation	Label	Displacement
[½½½] R_4^+	d_1	$O_I(y) = -O_{II}(z)$
[½½½] R_4^+	d_1	$O_I(x) = -O_{III}(z)$
[½½½] R_4^+	d_1	$O_{II}(x) = -O_{III}(y)$

$d_1 = au1$

3d

Space group	M_3^+	R_4^+	Tilts	Lattice vectors
$I2_1/b$ 11 (No. 15)	(0,0,0)	(a,a,c)	$a^-a^-c^-$	110 / 1$\overline{1}$0 / 002

Group generators: ½ + x, ½ + y, ½ + z; –x, y, ½ + z; –x, –y, –z

A	B		Cowley label	X
4e, u,½,¾	4b, 0,0,0		O_I	4e, u1,0,¼
			O_{II}, O_{III}	8f, ¼+u2,¼+v2,w2

Irreducible representation	Label	Displacement
[½½½] R_5^+	d_1	A(x)
[½½½] R_5^+	d_1	A(y)
[½½½] R_4^+	d_2	$O_I(y) = -O_{II}(z)$
[½½½] R_4^+	d_2	$O_I(x) = -O_{III}(z)$
[½½½] R_5^+	d_3	$O_{II}(x) = -O_{III}(y)$
[½½½] R_5^+	d_4	$O_I(y) = O_{II}(z)$
[½½½] R_5^+	d_4	$O_I(x) = O_{III}(z)$
[½½½] R_3^+	d_5	$O_{II}(x) = -O_{III}(x)$

$r_1 = au/\sqrt{2}$, $r_2 = au1/\sqrt{2}$, $r3 = \sqrt{2}au2$, $r4 = \sqrt{2}bv2$, $r_5 = cw2$
$M_{11} = M_{22} = M_{24} = M_{35} = M_{43} = M_{45} = M_{54} = 1$; $M_{33} = M_{82} = -1$
$Mi_{11} = 1$; $Mi_{22} = Mi_{34} = Mi_{42} = Mi_{45} = Mi_{53} = Mi_{54} = 1/2$; $Mi_{25} = Mi_{33} = -1/2$

3e

Space group	M_3^+	R_4^+	Tilts	Lattice vectors
$I11\,2_1/n$ (No. 12)	(0,0,0)	(a,b,0)	$a^-b^-c^0$	110 / 1$\overline{1}$0 / 002

Group generators: ½ + x, ½ + y, ½ + z; x, y, ½ – z; –x, –y, –z;

A	B	Cowley label	X
4i, ½+u,v,¼	4e, 0,0,0	O_I	4i, u1,v1,¼
		O_{II}	4h, ¾,¼,w2
		O_{III}	4g, ¾,¾,w3

Irreducible representation	Label	Displacement
[½½½] R_5^+	d_1	A(x)
[½½½] R_5^+	d_1	A(y)
[½½¼] R_5^+	d_2	A(x)
[½½½] R_5^+	d_2	A(y)
[½½½] R_4^+	d_3	$O_I(y) = -O_{II}(z)$
[½½½] R_4^+	d_4	$O_I(x) = -O_{III}(z)$
[½½½] R_5^+	d_5	$O_I(y) = O_{II}(z)$
[½½½] R_5^+	d_6	$O_I(x) = O_{III}(z)$

$r_1 = au/\sqrt{2}$, $r_2 = bv/\sqrt{2}$, $r_3 = \sqrt{2}au1$, $r_4 = \sqrt{2}bv1$, $r_5 = cw2$, $r6 = cw3$
$M_{11} = M_{22} = M_{33} = M_{34} = M_{35} = M_{36} = M_{44} = M_{46} = M_{53} = M_{64} = 1$; $M_{43} = M_{45} = M_{55} = M_{66} = -1$
$Mi_{11} = Mi_{22} = 1$; $Mi_{36} = Mi_{46} = 1/2$; $Mi_{55} = Mi_{65} = -1/2$; $Mi_{33} = Mi_{43} = Mi_{44} = Mi_{63} = Mi_{64} = 1/4$; $Mi_{34} = Mi_{54} = -1/4$

3f

Space group	M_3^+	R_4^+	Tilts	Lattice vectors
$F\overline{1}$ (No. 2)	(0,0,0)	(a,b,c)	$a^-b^-c^-$	200 / 020 / 002

A	B	B'	Cowley label	X
8i, ¼+u,¼+v,¼+w	4a, 0,0,0	4g, ½,½,½	O_I	8i, u1,v1,¼+w1
			O_{II}	8i, u2, ¼+v2,w2
			O_{III}	8i, ¼+u3,v3,w3

Irreducible representation	Label	Displacement
[½½½] R_5^+	d_1	A(x)
[½½½] R_5^+	d_2	A(y)
[½½½] R_5^+	d_3	A(z)
[½½½] R_1^+	d_4	$O_I(z)=O_{II}(y)=O_{III}(x)$
[½½½] R_3^+	d_5	$-\frac{1}{2}O_I(z)=O_{II}(y)=O_{III}(x)$
[½½½] R_3^+	d_6	$O_{II}(y) = -O_{III}(x)$
[½½½] R_4^+	d_7	$O_I(y) = -O_{III}(z)$
[½½½] R_4^+	d_8	$O_I(x) = -O_{III}(z)$
[½½½] R_4^+	d_9	$O_{II}(x) = -O_{III}(y)$
[½½½] R_5^+	d_{10}	$O_I(y) = O_{II}(z)$
[½½½] R_5^+	d_{11}	$O_I(x) = O_{III}(z)$
[½½½] R_5^+	d_{12}	$O_{II}(x) = O_{III}(y)$

$r_1 = au$, $r_2 = bv$, $r_3 = cw$, $r_4 = au1$, $r_5 = bv1$, $r_6 = cw1$, $r_7 = au2$, $r_8 = bv2$, $r_9 = cw2$, $r_{10} = au3$, $r_{11} = bv3$, $r_{12} = cw3$
$M_{11} = M_{22} = M_{33} = M_{4\,11} = M_{67} = M_{5\,10} = M_{64} = M_{79} = M_{7\,12} = M_{84} = M_{85} = M_{88} = M_{9\,10} = M_{10\,4} = M_{10\,5} = M_{11\,12} = M_{12\,8} = M_{12\,11} = 1$; $M_{48} = M_{97} = M_{10\,6} = M_{11\,9} = -1$; $M_{65} = -2$
$Mi_{11} = Mi_{22} = Mi_{33} = 1$, $Mi_{68} = Mi_{75} = Mi_{8\,12} = Mi_{87} = Mi_{10\,5} = Mi_{10\,9} = Mi_{11\,4} = Mi_{11\,12} = Mi_{12\,7} = Mi_{12\,11} = 1/2$; $Mi_{6\,10} = Mi_{79} = Mi_{84} = Mi_{8\,11} = -1/2$; $Mi_{46} = Mi_{48} = Mi_{4\,10} = 1/3$; $Mi_{56} = Mi_{58} = Mi_{5\,10} = 1/6$

TABLES 4a–d. DECOMPOSITION OF THE ISOTROPY SUBGROUPS CONSISTENT WITH IN-PHASE AND ANTI-PHASE TILTING

4a

Space group	M_3^+	R_4^+	Tilts	Lattice vectors
$Cmcm$ (No. 63)	(0,0,c)	(0,b,0)	$a^0b^-c^+$	200 / 020 / 002

A	B		Cowley label	X
4c, 0,v,¼	8d, ¼,¼,0		O_I	8g, ¼+u1,¼+v1,¼
4c, 0,½+v′,¼			O_{II}	8e, ¼+u2,0,0
			O_{III}	8f, 0,¼+v3,w3

Irreducible representation	Label	Displacement	
[½½½] R_5^+	d_1	A(y)	
[00½] X_5^+	d_2	A(y)	
[½½½] R_4^+	d_3	$O_I(x) = -O_{III}(z)$	
[½½0] M_3^+	d_4	$O_I(x) = -O_{II}(y)$	
[00½] X_5^+	d_5	$O_I(y)$	
[½½½] R_5^+	d_6	$O_I(x) = O_{III}(z)$	
[½½0] M_4^+	d_7	$O_{II}(y) = O_{III}(y)$	

$r_1 = bv$, $r_2 = bv'$, $r_3 = au1$, $r_4 = bv1$, $r_5 = au2$, $r_6 = bv3$, $r_7 = cw3$
$M_{11} = M_{12} = M_{22} = M_{33} = M_{38} = M_{45} = M_{54} = M_{57} = M_{67} = M_{73} = 1$; $M_{12} = M_{94} = M_{66} = -1$
$Mi_{54} = 1$; $Mi_{11} = Mi_{21} = Mi_{22} = Mi_{33} = Mi_{37} = Mi_{45} = Mi_{63} = Mi_{75} = 1/2$; $Mi_{12} = Mi_{46} =$
$Mi_{67} = -1/2$

4b

Space group	M_3^+	R_4^+	Tilts	Lattice vectors
$Pbnm$ (No. 62)	(0,0,c)	(a,a,0)	$a^-a^-c^+$	110 / 1$\overline{1}$0 / 002

A	B		Cowley label	X
4c, u,½+v,¼	4b, 0,0,0		O_I	4c, u1,v1,¼
			O_{II}, O_{III}	8d, ¼+u2, ¼+v2,w2

Irreducible representation	Label	Displacement
[½½½] R_5^+	d_1	A(x)
[½½½] R_5^+	d_1	A(y)
[00½] X_5^+	d_2	A(x)
[00½] X_5^+	d_2	A(y)
[½½½] R_4^+	d_3	$O_I(y) = -O_{II}(z)$
[½½½] R_4^+	d_3	$O_I(x) = -O_{III}(z)$
[½½0] M_3^+	d_4	$O_{II}(x) = -O_{III}(y)$
[00½] X_5^+	d_5	$O_I(x)$
[00½] X_5^+	d_5	$O_I(y)$
[½½0] M_2^+	d_6	$O_{III}(x) = -O_{II}(y)$
[½½½] R_5^+	d_7	$O_I(y) = O_{II}(z)$
[½½½] R_5^+	d_7	$O_I(x) = O_{III}(z)$

$r_1 = au/\sqrt2$, $r_2 = bv/\sqrt2$, $r_3 = au1/\sqrt2$, $r_4 = bv1/\sqrt2$, $r_5 = \sqrt2au2$, $r_6 = \sqrt2bv2$, $r_7 = cw2$
$M_{11} = M_{22} = M_{33} = M_{45} = M_{56} = M_{64} = M_{66} = 1$; $M_{37} = M_{54} = M_{73} = M_{77} = -1$
$Mi_{11} = Mi_{22} = Mi_{54} = 1$; $Mi_{33} = Mi_{45} = Mi_{65} = Mi_{66} = 1/2$; $Mi_{37} = Mi_{45} = Mi_{73} = Mi_{77} = -1/2$

4c

Space group	M_3^+	R_4^+	Tilts	Lattice vectors
$P4_2/nmc$ (No. 137)	(a,a,0)	(0,0,c)	$a^+a^+c^-$	200 / 020 / 002

A	B		Cowley label	X
2a, ¾,¼,¾	8e, 0,0,0		O_I	8f, u1,−u1,¼
2b, ¾,¼,¼			O_{II}	8g, ¼,v2,w2
4d, ¼,¼,¼+w			O_{III}	8g, ¼,½+v3,½+w3

Irreducible representation	Label	Displacement
[0½0] X_5^+	d_1	A(z)
[½00] X_5^+	d_1	A(z)
[½0½] M_3^+	d_2	$O_{III}(z) = -O_I(x)$
[0½½] M_3^+	d_2	$O_{II}(z) = -O_I(y)$
[½½½] R_4^+	d_3	$O_I(x) = -O_{III}(y)$
[½0½] M_4^+	d_4	$O_{III}(z) = O_I(x)$
[0½½] M_4^+	d_4	$O_{II}(z) = O_I(y)$
[½½0] M_4^+	d_5	$O_{II}(x) = O_{III}(y)$
[½00] X_5^+	d_6	$O_{II}(z)$
[0½0] X_5^+	d_6	$O_{II}(z)$

$r_1 = cw/2$, $r_2 = au1$, $r_3 = av2$, $r_4 = cw2$, $r_5 = av3$, $r_6 = cw3$
$M_{11} = M_{35} = M_{42} = M_{46} = M_{64} = M_{66} = 1$; $M_{22} = M_{24} = M_{33} = M_{44} = M_{53} = M_{55} = M_{62} = -1$
$Mi_{11} = 1$; $Mi_{53} = Mi_{64} = Mi_{66} = 1/2$; $Mi_{22} = Mi_{33} = Mi_{35} = Mi_{42} = Mi_{55} = -1/2$; $Mi_{24} = Mi_{46} = 1/4$; $Mi_{26} = Mi_{44} = -1/4$

4d

Space group	M_3^+	R_4^+	Tilts	Lattice vectors
$P112_1/m$ (No. 11)	(0,0,c)	(a,b,0)	$a^-b^-c^+$	110 / 1$\overline{1}$0 / 002

A	B	B′	Cowley label	X
2e, u,½+v,¼	2a, 0,0,0	2d, ½,½,0	O_I	2e, u1,v1,¼
2e, ½+u′,v′,¼			O_I	2e, ½+u1′,½+v1′,¼
			O_{II}	4f, ¾+u2,¼+v2,½+w2
			O_{III}	4f, ¼+u3,¼+v3,w3

Irreducible representation	Label	Displacement
[½½½] R_5^+	d_1	A(x)
[½½½] R_5^+	d_1	A(y)
[00½] X_5^+	d_2	A(x)
[00½] X_5^+	d_2	A(y)
[½½½] R_5^+	d_3	A(x)
[½½½] R_5^+	d_3	A(y)
[00½] X_5^+	d_4	A(x)
[00½] X_5^+	d_4	A(y)
[½½½] R_4^+	d_5	$O_I(y) = -O_{II}(z)$
[½½½] R_4^+	d_6	$O_I(x) = -O_{III}(z)$
[½½0] M_3^+	d_7	$O_{II}(x) = -O_{III}(y)$
[00½] X_5^+	d_8	$O_I(x)$
[00½] X_5^+	d_9	$O_I(y)$
[½½0] M_2^+	d_{10}	$O_{III}(x) = -O_{II}(y)$
[½½½] R_5^+	d_{11}	$O_I(y) = O_{II}(z)$
[½½½] R_5^+	d_{12}	$O_I(x) = O_{III}(z)$
[½½0] M_4^+	d_{13}	$O_{II}(x) = O_{III}(y)$
[½½0] M_1^+	d_{14}	$O_{III}(x) = O_I(y)$

$r_1 = au/\sqrt2$, $r_2 = bv/\sqrt2$, $r_3 = au'/\sqrt2$, $r_4 = bv'/\sqrt2$, $r_5 = \sqrt2au1$, $r_6 = \sqrt2bv1$, $r_7 = \sqrt2au1'$, $r_8 = \sqrt2bv1'$, $r_9 = \sqrt2au2$, $r_{10} = \sqrt2bv2$, $r_{11} = cw2$, $r_{12} = \sqrt2au3$, $r_{13} = \sqrt2bv3$, $r_{14} = cw3$

$M_{11} = M_{24} = M_{43} = M_{44} = M_{55} = M_{56} = M_{58} = M_{66} = M_{68} = M_{69} = M_{6\,11} = M_{76} = M_{7\,11} = M_{7\,12} = M_{85} = M_{89} = M_{8\,12} = M_{9\,10} = M_{9\,13} = M_{9\,14} = M_{10\,13} = M_{12\,10} = M_{13\,7} = M_{13\,10} = M_{13\,13} = 1$; $M_{12} = M_{23} = M_{31} = M_{32} = M_{59} = M_{5\,11} = M_{5\,12} = M_{65} = M_{6\,12} = M_{75} = M_{78} = M_{79} = M_{86} = M_{8\,11} = M_{97} = M_{10\,7} = M_{10\,10} = M_{10\,14} = M_{11\,5} = M_{11\,11} = M_{12\,7} = M_{12\,13} = M_{12\,14} = M_{13\,14} = M_{14\,8} = M_{14\,12} = -1$

$Mi_{11} = Mi_{34} = Mi_{42} = Mi_{44} = 1/2$; $Mi_{13} = Mi_{21} = Mi_{23} = Mi_{5\,11} = Mi_{6\,14} = Mi_{11\,11} = Mi_{12\,14} = -1/2$; $Mi_{7\,13} = Mi_{85} = Mi_{86} = Mi_{87} = Mi_{94} = Mi_{98} = Mi_{10\,9} = Mi_{10\,12} = Mi_{10\,13} = Mi_{13\,9} = Mi_{13\,10} = Mi_{13\,13} = Mi_{14\,9} = 1/4$; $Mi_{79} = Mi_{7\,10} = Mi_{7\,12} = Mi_{95} = Mi_{97} = Mi_{10\,10} = Mi_{13\,12} = Mi_{14\,10} = Mi_{14\,12} = Mi_{14\,13} = -1/4$; $Mi_{55} = Mi_{58} = Mi_{65} = Mi_{66} = Mi_{11\,5} = Mi_{11\,7} = Mi_{12\,7} = Mi_{12\,8} = 1/8$; $Mi_{56} = Mi_{57} = Mi_{67} = Mi_{68} = Mi_{11\,5} = Mi_{11\,8} = Mi_{12\,5} = Mi_{12\,6} = -1/8$

Ambient-temperature structural parameters for $CaTiO_3$, derived from a two-bank Rietveld fit to neutron time-of-flight data collected using HRPD at ISIS, are listed in the non-italicized text in Table 5, with Figure 3 showing the quality of the fit to these data. Using these results and those in Table 4b for the elements of $\mathbf{M^{-1}}$, the magnitudes of the *sabv* in Å are therefore

$$
\begin{pmatrix}
1 & 0 & 0 & 0 & 0 & 0 & 0 \\
0 & 1 & 0 & 0 & 0 & 0 & 0 \\
0 & 0 & 0.5 & 0 & 0 & 0 & -0.5 \\
0 & 0 & 0 & 0 & -0.5 & 0.5 & 0 \\
0 & 0 & 0 & 1 & 0 & 0 & 0 \\
0 & 0 & 0 & 0 & 0.5 & 0.5 & 0 \\
0 & 0 & -0.5 & 0 & 0 & 0 & -0.5
\end{pmatrix}
\begin{pmatrix}
au/\sqrt{2} \\
bv/\sqrt{2} \\
au1/\sqrt{2} \\
bv1/\sqrt{2} \\
\sqrt{2}au2 \\
\sqrt{2}bv2 \\
cw2
\end{pmatrix}
=
\begin{pmatrix}
d_1 \\
d_2 \\
d_3 \\
d_4 \\
d_5 \\
d_6 \\
d_7
\end{pmatrix}
=
\begin{pmatrix}
0.0234(4) \\
0.1361(3) \\
-0.279(1) \\
0.301(2) \\
-0.0621(3) \\
-0.0005(20) \\
-0.005(1)
\end{pmatrix}
$$

where it can be seen that the *A*-site displacement (d_1, d_2) is dominated by the *sabv* with *irrep* [0 0 ½] X_5^+ (d_2), whereas the anion displacements ($d_3 - d_7$) are dominated by the two tilt modes with *irreps* [½ ½ ½] R_4^+ (d_3) and [½ ½ 0] M_3^+ (d_4) and, to a lesser extent, the octahedral deformation mode with *irrep* [0 0 ½] X_5^+ (d_5). The *sabv* $X_{III}(x) = -X_{II}(y)$ with *irrep* M_2^- (d_6) is zero within the estimated standard deviation.

With the exceptions of the tilt systems $a^0a^0c^+$ (*P4/mbm*), $a^0a^0c^-$ (*I4/mcm*) and $a^-a^-a^-$ (*F$\bar{3}$2/n*), in which the octahedra may be deformed but not distorted [see Megaw & Darlington (1975) for an explanation of the differences between these two terms] and from which the tilt angles can be calculated through simple trigonometry, all other tilt systems permit the complication of both deformation and distortion of the BX_6 octahedron. The usual methods for the determinations of the tilt angles within these more complex tilt systems, often calculated using $B - X - B$ bond angles, are generally approximations, and their evaluation can become a significant problem in low-symmetry space-groups

(Tamazyan & van Smaalen 2007). The major advantage of decomposing the perovskite structure in terms of *sabvs* is that it uniquely allows the precise determination of the tilt angles of the octahedron free from the effects of octahedron distortion. The individual tilt-angle component can be calculated as the arc tangent of the octahedral displacement to half the magnitude of either of the pseudocubic lattice constants normal to the tilt axis. Alternatively, and to an excellent approximation by averaging over all pseudocubic lattice constants, this angle can be calculated by

TABLE 5. THE CRYSTAL STRUCTURE OF CaTiO₃ AT ROOM TEMPERATURE USING THE FULL NUMBER OF DEGREES OF FREEDOM PERMITTED BY THE SPACE GROUP (NORMAL TEXT) AND WITH THE CONTRIBUTION OF THE SYMMETRY-ADAPTED BASIS-VECTOR WITH IRREDUCIBLE REPRESENTATION M_2^- SET TO ZERO (ITALIC TEXT)

Atom	x	y	z	$100u_{iso}$ / Å² (or $100u_{eq}$ / Å²)
Ca	0.0061(2)	0.5354(2)	0.25	1.01(2)
	0.0061(2)	*0.5354(2)*	*0.25*	*1.01(2)*
Ti	0.0	0.0	0.0	0.85(2)
	0.0	*0.0*	*0.0*	*0.85(2)*
O1	-0.0719(1)	-0.0162(1)	0.25	0.92(5)
	-0.0720(1)	*-0.0162(1)*	*0.25*	*0.92(5)*
O2	0.2104(1)	0.2891(1)	0.0372(1)	0.93(3)
	0.21044(6)	*0.28916(6)*	*0.03720(7)*	*0.93(3)*

a = 5.38095(2) Å,	b = 5.43710(2) Å,	c = 7.64208(5) Å
Rp = 0.036,	Rwp = 0.039,	χ^2 = 4.457 for 39 variables
a = 5.38095(2) Å,	*b = 5.43710(2) Å,*	*c = 7.64208(5) Å*
Rp = 0.036,	*Rwp = 0.039,*	*χ^2 = 4.457 for 38 variables*

FIG. 3. Two-bank Rietveld refinement of $CaTiO_3$ perovskite at room temperature. The upper difference plot in both figures is derived from a refinement based on the full structural degrees of freedom permitted for such a structure in space group *Pbnm*, whereas the lower difference curve is derived from a refinement with the contribution of the symmetry-adapted basis-vector with irreducible representation M_2^- set to zero, *i.e.*, with one less structural degree of freedom.

$$\phi_R = \arctan\left(2\left(\frac{N}{V}\right)^{1/3} R_4^+\right)$$

$$\phi_M = \arctan\left(2\left(\frac{N}{V}\right)^{1/3} M_3^+\right)$$

where ϕ_R and ϕ_M are the magnitudes of the anti- and in-phase tilt angles respectively, R_4^+/M_3^+ is the magnitude of the corresponding displacement, V is the unit-cell volume, and N is the number of primitive aristotype unit cells in volume V. The total angle of tilt of either type is given by the square root of the sum of the squares of the individual tilts of that particular type.

For crystallographic studies of perovskites as a function of temperature, pressure or applied electric or magnetic fields, the decomposition of the crystal structures in terms of the magnitudes of orthogonal basis-vectors presents an alternative crystal-chemical analysis strategy to the conventional techniques of studying variations in bond lengths and angles. Note that as the deviation of the fractional coordinates from ideality are simply linear combinations of *sabvs*, the magnitude of bond lengths, bond angles and polyhedron volumes can be written as a function of the lattice parameters and the *sabvs* amplitudes, taking into account the associated sign.

The rapid data-collection protocols used in parametric studies where a great many data-points are collected as a function of one or more thermodynamic variables are particularly suited to this kind of analysis. In parametric studies, high structural precision at a limited number of points in thermodynamic space is sacrificed for more detailed trends at significantly lower precision. Variables that can be physically parameterized, *e.g.*, the temperature dependence of the atomic displacement parameters in $KMgF_3$ perovskite according to a Debye model (Wood *et al.* 2002) can be replaced by their fitted values, and the structure refinement re-iterated. In general, the estimated standard deviations of the non-parametrizable variables are improved using this method (Sivia 1996), thus leading to improvements in the precision of the structural trends. A great many rapid collections of data at high resolution have been made by Darlington, Howard and Kennedy and their coworkers (Darlington *et al.* 1994, 2003, 2005, Darlington & Knight 1994, 1999a, 1999b, Howard *et al.* 2000, 2002, 2007, Forrester *et al.* 2006, Kennedy *et al.* 2006, Carpenter *et al.* 2005, 2006, Zhang *et al.* 2006, 2007a, 2007b) to investigate the temperature dependence of the spontaneous strain, angles of octahedron tilt and ferroelectric displacements. One significant advantage of the *sabv* decomposition in parametric Rietveld studies is that it allows Occam's razor to be applied in a statistically justifiable manner. If it is assumed that covariance terms are smaller than variance

terms, then it is possible to estimate errors in the *sabvs* magnitudes using standard statistical methods (Sivia 1996) simply by using derived, or published, estimated standard deviations of the structural parameters:

$$\left(\sigma_p^2 = \sum_q N_{pq}^2 \sigma_q^2\right).$$

If a data-collection protocol is followed where at least some of the data are collected long enough to allow precise structural parameters to be determined at a few points, these results can be decomposed into *sabvs*, and estimated errors can be assigned to each. If a *sabv* is found to be zero within esd, it can be set to zero and the coordinates can be recast taking the absence of this mode into account, thereby reducing the number of degrees of freedom in the crystal-structure refinement. If the space group *Pbnm* is taken as an example, should the *sabv* with *irrep* [0 0 ½] X_5^+ (d_5) have zero magnitude, then the y coordinate of O1 would be fixed at zero in the subsequent re-refinement of the crystal structure. In the particular case of $CaTiO_3$ at room temperature, decomposition found that the *sabv* $X_{III}(x) = -X_{II}(y)$ with *irrep* M_2^+ (d_6) is zero within estimated standard deviation. Setting the contribution of this mode to zero by the application of linear constraints, *i.e.*, reducing the effective number of variables in the least-squares refinement by one, the model was re-refined, giving rise to the results shown in italics in Table 5. At the statistical quality of the data recorded, the crystallographic results and agreement factors listed in Table 5 show that the anion-displacement pattern from this mode is not present in the crystal structure at room temperature. This result is in accordance with the conclusions drawn by Cochran & Zia (1968) based on their analysis of unpublished single-crystal X-ray-diffraction results for $CaTiO_3$. Hence, as this mode corresponds to a secondary-order parameter, and will reduce in magnitude with increasing temperature, it would be safe to set its contribution to zero in any future high-temperature parametric study of $CaTiO_3$ in the phase with space group *Pbnm*.

Using the commonly available Rietveld software, it might not be possible to derive the correct set of linear constraints in significantly more complex cases than these; it should be possible, however, to program the crystal-structure refinement in terms of *sabvs* using the sophisticated algorithms employed in the new generation of Rietveld refinement software such as TOPAS (Kern & Coelho 1998).

As a final demonstration of the method, the decomposition of the crystal structure of $KCaF_3$ as a function of temperature between 4.2 and 542 K in the orthorhombic *Pbnm* phase is briefly described, as a more detailed analysis will be published elsewhere. The phase $KCaF_3$ undergoes two first-order structural phase-transitions, at 560 K from the aristotype to an ortho-
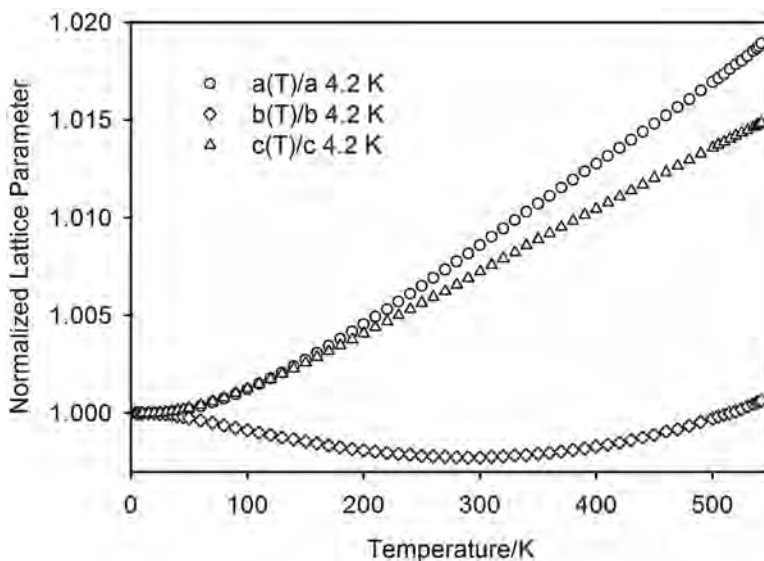
FIG. 4. The temperature dependence of the normalized lattice-parameters of $KCaF_3$ between 4.2 and 542 K in the orthorhombic phase with space group *Pbnm*. The lattice parameters *a* and *c* show the typical expected Grüneisen behavior, whereas the *b* axis shows an unusual region of negative thermal expansion between 15 and 300 K.

rhombic structure with space group *Cmcm* ($a^0b^-c^+$), and at 551 K to an orthorhombic structure with space group *Pbnm* ($a^-a^-c^+$) (Bulou *et al*. 1980, Knight *et al*. 2005b). High-resolution powder neutron-diffraction data were collected using HRPD at ISIS at 4.2 K, then at 10 K to 50 K in 5 K steps, from 60 K to 500 K in 10 K steps, from 505 K to 535 K in 5 K steps, and finally from 538 K to 574 K in 2 K steps. Long periods of data collection, approximately two hours in duration, were made at 4.2 K, 25 K, 50 K and 50 K intervals to 500 K, then at 525 K, 542 K, 566 K and 568 K. All other data collections were approximately fifteen minutes in duration.

Figure 4 shows the lattice-parameter variations with temperature, normalized to their values at 4.2 K (estimated standard deviations for each crystallographic axis are smaller than the plotting symbols used). Using expressions derived by O'Keefe & Hyde (1977) for the lattice constants of perovskites as a function of tilt angle, it can easily be shown for regular tilted octahedra in space group *Pbnm* that

$$\frac{1}{b}\frac{db}{dT} = \frac{1}{a}\frac{da}{dT} - \frac{1}{c}\frac{dc}{dT}$$

applies. Knight *et al*. (2005b) have pointed out that the CaF_6 octahedron in $KCaF_3$ has a significant temperature-dependent distortion between 4.2 K and 300 K, and hence this expression is not even approximately

obeyed over the temperature interval measured; this is in contrast to the almost ideal behavior of the protonic conductor $SrCe_{0.95}Yb_{0.05}O_\xi$ ($\xi \approx 3$) between 373 and 1273 K (Knight *et al*., in prep.). Consideration of Figure 4 shows that the *b* axis exhibits negative thermal expansion from 15 K to ~300 K, and only recovers the value it had at 4.2 K by about 500 K. The *a* and *c* axes, in contrast, exhibit the expected Grüneisen behavior of saturation at low temperature, an increase with increasing temperature and a constant coefficient of thermal expansion at higher temperatures.

Figures 5a–g shows the magnitudes of the seven symmetry-adapted basis-vectors within the ortho-rhombic *Pbnm* phase. The behavior of the K cation, shown in Figures 5a and 5b, is dominated by the displacement associated with the *sabv* A(x) with *irrep* X_5^+ (d_2), for which the reduction with temperature is approximately 4.5 times larger than that for the *sabv* A(x) with *irrep* R_5^+ (d_1). The magnitudes of the *sabvs* extrapolate to zero at ~790 K for d_1 and ~700 K for d_2, both significantly higher than the phase-transition temperature to the cubic phase.

The magnitudes of the two displacements associated with the tilting of the octahedra are shown in Figures 5c and 5d. At 4.2 K, the two tilt components have similar magnitudes, but with increasing temperature, the anti-phase tilt shows only a limited saturation region, of the order of 50 K, before reducing rapidly. The in-phase tilt by comparison has a much larger region of saturation, of
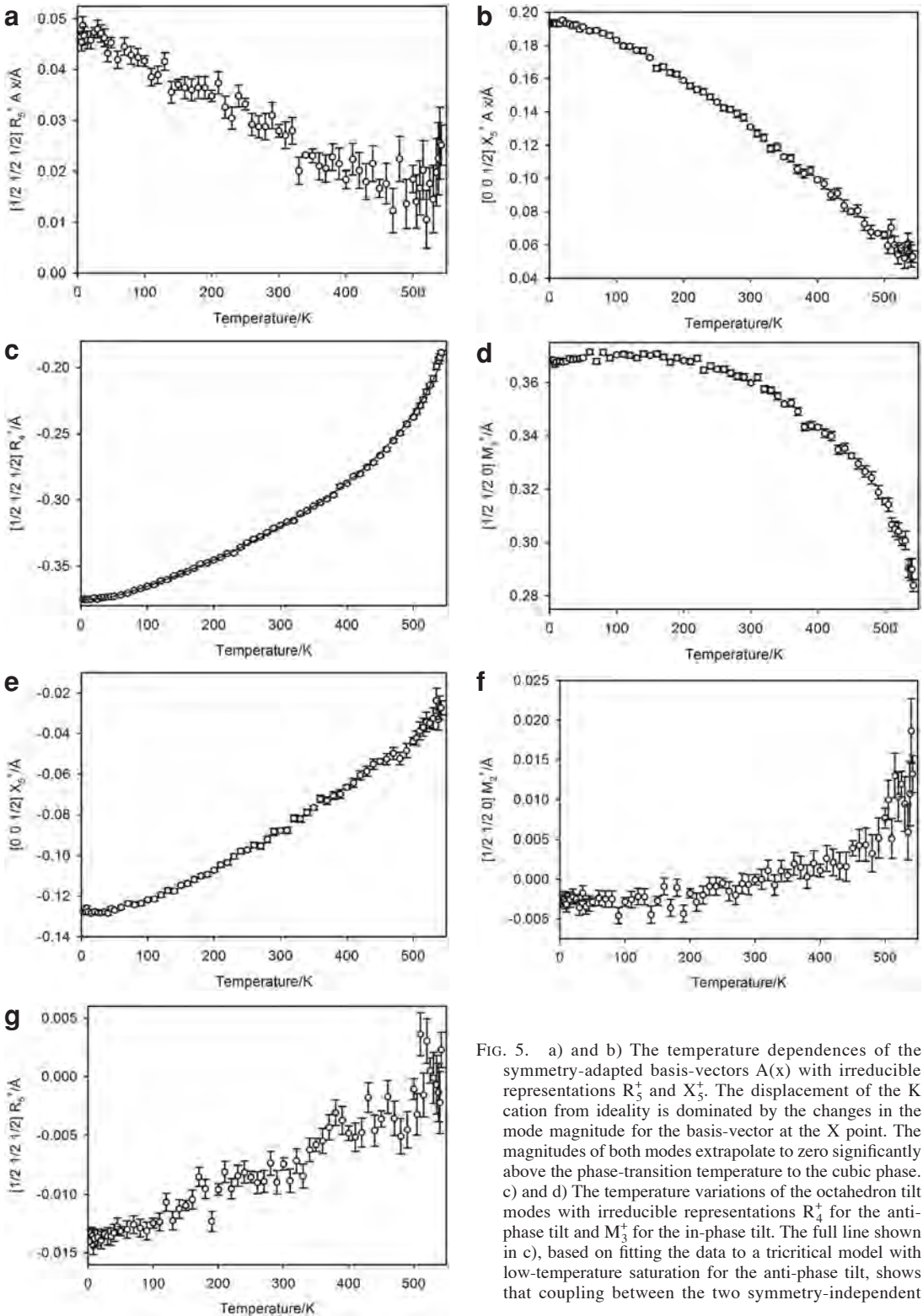
FIG. 5. a) and b) The temperature dependences of the symmetry-adapted basis-vectors A(x) with irreducible representations R_5^+ and X_5^+. The displacement of the K cation from ideality is dominated by the changes in the mode magnitude for the basis-vector at the X point. The magnitudes of both modes extrapolate to zero significantly above the phase-transition temperature to the cubic phase. c) and d) The temperature variations of the octahedron tilt modes with irreducible representations R_4^+ for the anti-phase tilt and M_3^+ for the in-phase tilt. The full line shown in c), based on fitting the data to a tricritical model with low-temperature saturation for the anti-phase tilt, shows that coupling between the two symmetry-independent

the order of ~200 K, and exhibits a slower decrease with temperature. Using Landau theory, taking into account the theoretical coupling that could exist between the two modes, Carpenter (2007) has shown that the magnitudes of these displacements are related *via* a pair of non-linear simultaneous equations.

$$\frac{\partial G}{\partial q_4} = 0 = 2a_2 \Theta_{s2} \left[\coth\left(\frac{\Theta_{s2}}{T}\right) - \coth\left(\frac{\Theta_{s2}}{T_{c2}}\right) \right]$$
$$+ 2b_2 q_4^2 + 4c_2 q_4^4 + 4\lambda^* q_2^2 + \frac{4\lambda_5^2 (\lambda_6 + \lambda_7) q_2^2 q_4^2}{C_{44}^{0\ 2}}$$

$$\frac{\partial G}{\partial q_2} = 0 = a_1 \Theta_{s1} \left[\coth\left(\frac{\Theta_{s1}}{T}\right) - \coth\left(\frac{\Theta_{s1}}{T_{c1}}\right) \right]$$
$$+ b_1 q_2^2 + c_1 q_2^4 + 4\lambda^* q_4^2 + \frac{2\lambda_5^2 (\lambda_6 + \lambda_7) q_4^2}{C_{44}^{0\ 2}}$$

where q_2 is the order parameter associated with the *irrep* M_3^+, q_4 is the order parameter associated with the *irrep* R_4^+, T_{c1}, T_{c2} are critical temperatures, Θ_{s1}, Θ_{s2} are saturation temperatures, a_1, a_2 are normal Landau coefficients, b_1, b_2, c_1, c_2 are renormalized Landau coefficients; λ^*, λ_5, λ_6, λ_7 are coupling coefficients and C_{44}^0 is the bare elastic constant of the cubic phase. Despite evidence from inelastic neutron scattering, which finds the whole of the line $\left[\frac{1}{2} \frac{1}{2} \xi\right]$ in reciprocal space to be soft (Rousseau *et al.* 1997), the fit to the data shown as the full line in Figure 5c is derived from the simplest possible assumptions, namely that the coupling between the two modes is negligible, and that the term b_2 is zero.

The behavior of the anti-phase tilt is therefore close to tricritical in behavior, with a saturation temperature Θ_{s2} of 58(2) K and a critical temperature T_{c2} of 580(1) K. The low-temperature region for the in-phase tilt appears to show a counterintuitive reduction in magnitude with decreasing temperature and is the subject of continuing work.

modes is small. e)–g) The temperature dependencies of the octahedron-distortion modes in KCaF$_3$. The distortion is dominated principally by the symmetry-adapted basis-vector with irreducible representation X_5^+, with a minor role being played by the basis-vector with irreducible representation R_5^+. The octahedron distortion mode with irreducible representation M_2^+ is finite but very small at low temperatures in KCaF$_3$, in contrast to CaTiO$_3$, where it is found to be zero within the estimated standard deviation at room temperature.

The distortion of the CaF$_6$ octahedron mediated by *sabvs* with *irreps* X_5^+, M_2^+ and R_5^+ is shown in Figures 5e–g. The dominant distortion arises from *sabv* with *irrep* X_5^+, which is a factor of nearly nine times larger than the magnitude of the *sabv* with *irrep* R_5^+. By 500 K, the *sabv* with *irrep* R_5^+ has negligible magnitude. For temperatures below ~400 K, the *sabv* with *irrep* M_2^+ differs from zero by about two estimated standard deviations, unlike the case of CaTiO$_3$, where it was found to be zero at room temperature. At temperatures greater than 400 K, it could be argued that this *sabv* has zero magnitude and that the structural model could be re-refined testing this hypothesis. Taking into account the strong temperature-dependence of the *sabv* with *irrep* X_5^+ and, to a lesser extent, the weaker temperature-dependence of the *sabv* with *irrep* R_5^+, it is hardly surprising to find that the axial thermal expansion coefficients do not obey the simple relationship expected of ideal, regular octahedra.

CONCLUSIONS

Centrosymmetric perovskite (ABX$_3$) hettotypes, derived from the tilting of the constituent BX$_6$ octahedra from the cubic aristotype phase, show two major structural characteristics. The first is the facile observation that the coordination at the *B* site remains octahedral in all hettotype phases, although the observed symmetry is frequently far from the ideal point-symmetry, $m\bar{3}m$, of the aristotype phase. The second is that the *A* site shows a lower coordination-number than the twelve it exhibits in the aristotype phase; furthermore, the coordination polyhedron is generally of a complex shape. Tilting of the octahedra occurs because the ionic radius of the *A*-site cation is too small with respect to that of the *B*-site cation to stabilize the aristotype structure. Rotation(s) of the octahedra permits the *B*-site cation to remain sixfold-coordinated while reducing the bond lengths to the *A*-site cation to acceptable lengths. Crystallographic data for perovskite-structured phases as a function of a thermodynamic variable are generally interpreted in terms of the bond lengths and angles of the two constituent coordination-polyhedra. Whereas this analysis is generally simple to carry out for the *B* site, the interpretation of the *A*-site geometry is generally far from clearcut. An alternative methodology for crystallographic interpretation is to decompose the crystal structure of the perovskite hettotype into a set of frozen normal-mode amplitudes, the magnitudes of the symmetry-adapted basis-vectors. From these, the details of the structural distortions at both sites can readily be interpreted. These ideas are far from new, however; they were originally developed in the late 1960s by Cochran & Zia (1968) in a lattice dynamics, rather than crystallographic, context. The bridge between the lattice dynamics interpretation of Cochran & Zia (1968) and its real potential for use in a crystallographic interpretation was first made by Darlington (2002a,

2002b). In the work reported in this paper, the method for parameterizing all fourteen space-groups consistent with zone-boundary tilting of the BX_6 octahedra has been reported. The potential of the method for either the precise characterization of structure from high-quality crystallographic data, or as an aid in the study of structural trends from rapidly collected parametric data, has been outlined and illustrated by examples.

Using the large number of well-characterized perovskite crystal structures, it would be interesting to test whether the magnitudes of the associated symmetry-adapted basis-vectors show particularly simple relationships to the basic crystal-chemical variables, such as ionic radii, tolerance factors or electronegativities. Should this be so, provided the unit-cell metric and space group are known, one may also have the ability to predict the crystal structure of perovskite phases using this form of structural parameterization.

ACKNOWLEDGEMENTS

REFERENCES

BRADLEY, C.J. & CRACKNELL, A.P. (1972): *The Mathematical Theory of Symmetry in Solids: Representation Theory for Point Groups and Space Groups*. Clarendon Press, Oxford., U.K.

BULOU, A., NOUET, J., HEWAT, A.W. & SCHÄFER, F.J. (1980): Structural phase transitions in $KCaF_3$ - DSC, birefringence and neutron powder diffraction results. *Ferroelectrics* **25**, 375-378.

CARPENTER, M.A. (2007): Elastic anomalies accompanying phase transitions in $(Ca,Sr)TiO_3$ perovskites. I. Landau theory and a calibration for $SrTiO_3$. *Am. Mineral.* **92**, 309-327.

CARPENTER, M.A., HOWARD, C.J., KENNEDY, B.J. & KNIGHT, K.S. (2005): Strain mechanism for order-parameter coupling through successive phase transitions in $PrAlO_3$. *Phys. Rev. B* **72**, 024118.

CARPENTER, M.A., HOWARD, C.J., KNIGHT, K.S. & ZHANG, Z. (2006): Structural relationships and a phase diagram for $(Ca,Sr)TiO3$ perovskites. *J. Phys.: Condens. Matter* **18**, 10725-10749.

COCHRAN, W. & ZIA, A. (1968): Structure and dynamics of perovskite-type crystals. *Phys. Status Solidi* **25**, 273-283.

COWLEY, R.A. (1964): Lattice dynamics and phase transitions of strontium titanate. *Phys. Rev.* **134**, A981-A997.

DAOUD-ALADINE, A., MARTIN. C., CHAPON, L.C., HERVIEU, M., KNIGHT, K.S., BRUNELLI, M. & RADAELLI, P.G. (2007): Structural phase transition and magnetism in hexagonal $SrMnO_3$ by magnetization measurements and by electron, X-ray, and neutron diffraction studies. *Phys. Rev. B* **75**, 104417.

DARLINGTON, C.N.W. (2002a): Normal-mode analysis of the structures of perovskites with tilted octahedra. *Acta Crystallogr.* A**58**, 66-71.

DARLINGTON, C.N.W. (2002b): Normal-mode analysis of the structures of perovskites with tilted octahedra. Erratum. *Acta Crystallogr.* A**58**, 299-300.

DARLINGTON, C.N.W., DAVID, W.I.F. & KNIGHT, K.S. (1994): Structural study of barium titanate between 150 and 425 K. *Phase Transitions* **48**, 217-236.

DARLINGTON, C.N.W., HRILJAC, J.A. & KNIGHT, K.S. (2003): Structures of $Na_{0.74}WO_3$. *Acta Crystallogr.* B**59**, 584-587.

DARLINGTON, C.N.W., HRILJAC, J.A. & KNIGHT, K.S. (2005): Temperature dependence of structural parameters in the perovskite $Na_{0.74}WO_3$. *Phys. Status Solidi (B)* **242**, 854-868.

DARLINGTON, C.N.W. & KNIGHT, K.S. (1994): Structural study of potassium niobate between 200 and 823 K. *Phase Transitions* **52**, 261-275.

DARLINGTON, C.N.W. & KNIGHT, K.S. (1999a): High temperature phases of $NaNbO_3$ and $NaTaO_3$. *Acta Crystallogr.* B**55**, 24-30.

DARLINGTON, C.N.W. & KNIGHT, K.S. (1999b): On the lattice parameters of sodium niobate at room temperature and above. *Physica B* **266**, 368-372.

FORRESTER, J.S., KISI, E.H., KNIGHT, K.S. & HOWARD, C.J. (2006): Rhombohedral to cubic phase transition in the relaxor ferroelectric PZN. *J. Phys.: Condens. Matter* **18**, L233-L240.

GLAZER, A.M. (1972): The classification of tilted octahedra in perovskites. *Acta Crystallogr.* B**28**, 3384-3392.

GLAZER, A.M. (1975): Simple ways of determining perovskite structures. *Acta Crystallogr.* **A31**, 756-762.

HOWARD, C.J., KENNEDY, B.J. & WOODWARD, P.M. (2003): Ordered double perovskites – a group-theoretical analysis. *Acta Crystallogr.* **B59**, 463-471.

HOWARD, C.J., KNIGHT, K.S., KENNEDY, B.J. & KISI, E.H. (2000): The structural phase transitions in strontium zirconate revisited. *J. Phys.: Condens. Matter* **12**, L677-L683.

HOWARD, C.J., LUCA, V. & KNIGHT, K.S. (2002): High-temperature phase transitions in tungsten trioxide – the last word? *J. Phys.: Condens. Matter* **14**, 377-387.

HOWARD, C.J. & STOKES, H.T. (1998): Group-theoretical analysis of octahedral tilting in perovskites. *Acta Crystallogr.* **B54**, 782-789.

HOWARD, C.J. & STOKES, H.T. (2002): Group-theoretical analysis of octahedral tilting in perovskites. Erratum. *Acta Crystallogr.* **B58**, 565.

HOWARD, C.J. & STOKES, H.T. (2005): Structures and phase transitions in perovskites – a group theoretical approach. *Acta Crystallogr.* **A61**, 93-111.

HOWARD, C.J. & ZHANG, ZHAOMING (2004a): Structure for perovskites with layered ordering of the *A*-site cations. *Acta Crystallogr.* **B60**, 249-251.

HOWARD, C.J. & ZHANG, ZHAOMING (2004b): Structure for perovskites with layered ordering of the *A*-site cations. Erratum. *Acta Crystallogr.* **B60**, 763.

HOWARD, C.J., ZHANG, ZHAOMING, CARPENTER, M.A. & KNIGHT, K.S. (2007): Suppression of strain coupling in perovskite $La_{0.6}Sr_{0.1}TiO_3$ by cation disorder. *Phys. Rev. B* **76**, 054108.

KENNEDY, B.J., HOWARD, C.J., KNIGHT, K.S., ZHANG, ZHAOMING & ZHOU, QINGDI (2006): Structures and phase transitions in the ordered double perovskites $Ba_2Bi^{III}Bi^VO_6$ and $Ba_2Bi^{III}Sb^VO_6$. *Acta Crystallogr.* **B62**, 537-546.

KERN, A.A. & COELHO, A.A. (1998): TOPAS version 2.1: *General Profile and Structure Analysis Software for Powder Diffraction Data.* Bruker AXS, Karlsruhe, Germany.

KNIGHT, K.S. (1994): Structural phase transitions in $BaCeO_3$. *Solid State Ionics* **74**, 109-117.

KNIGHT, K.S. (2001): Structural phase transitions, oxygen vacancy ordering and protonation in doped $BaCeO_3$: results from time-of-flight neutron powder diffraction investigations. *Solid State Ionics* **145**, 275-294.

KNIGHT, K.S. (2009): Parameterization of centrosymmetric elpasolite crystal structures in terms of symmetry-adapted basis-vectors of the primitive cubic aristotype phase. *Can. Mineral.* **47**, 401-420.

KNIGHT, K.S., DARLINGTON, C.N.W. & WOOD, I.G. (2005b): The crystal structure of $KCaF_3$ at 4.2 and 300K: a re-eval-

uation using high-resolution powder neutron diffraction. *Powder Diffraction* **20**, 7-13.

KNIGHT, K.S., MARSHALL, W.G., BONANOS, N. & FRANCIS, D.J. (2005a): Pressure dependence of the crystal structure of $SrCeO_3$ perovskite. *J. Alloys Compounds* **394**, 131-137.

KOSTER, G.F. (1957): Space groups and their representations. *Solid State Phys.* **5**, 173-256.

LANDAU, L.D. & LIFSHITZ, E.M. (1996): *Statistical Physics* (3rd ed.). Butterworth–Heinemann, Oxford., U.K.

LEINENWEBER, K. & PARISE, J.B. (1995): High pressure synthesis and crystal structure of $CaFe_2TiO_6$, a new perovskite structure type. *J. Solid State Chem.* **114**, 277-281.

LUFASO, M.W. & WOODWARD, P.M. (2001): Prediction of crystal structures of perovskites using the software SPuDS. *Acta Crystallogr.* **B57**, 725-738.

MEGAW, H.D. & DARLINGTON, C.N.W. (1975): Geometrical and structural relations in rhombohedral perovskites. *Acta Crystallogr.* **A31**, 161-173.

MITCHELL, R.H. (2002): *Perovskites Modern and Ancient,* Almaz Press, Thunder Bay, Ontario.

MITCHELL, R.H., ALEXANDER, M., CRANSWICK, L.M.D. & SWAINSON, I.P. (2007): A powder neutron diffraction study of the crystal structure of the fluoroperovskite $NaMgF_3$ (neighborite) from 300 to 3.6 K. *Phys. Chem. Minerals* **34**, 705-712.

MONTGOMERY, H. (1969): The symmetry of lattice vibrations in the zinc blende and diamond structures. *Proc. R. Soc. A* **309**, 521-549.

O'KEEFE, M. & HYDE, B.G. (1977): Some structures topologically related to cubic perovskites ($E2_1$), ReO_3 ($D0_9$) and Cu_3Au ($L1_2$). *Acta Crystallogr.* **B33**, 3802-3813.

RANLØV, J. (1995): *Perovskite-Type Metal Oxides. Electrical Conductivity and Structure.* Risø-R-796(EN), Risø National Laboratory, Roskilde, Denmark.

ROSS, N.L. & HAZEN, R.M. (1989): Single crystal X-ray diffraction study of $MgSiO_3$ perovskite from 77 to 400 K. *Phys. Chem. Minerals* **16**, 415-420.

ROUSSEAU, M., DANIEL, P. & HENNION, B. (1997): The dynamic signature of highly anisotropic correlation near the phase transition in $KCaF_3$. *J. Phys.: Condens. Matter* **9**, 8963-8971.

SIVIA, D.S. (1996): *Data Analysis, a Bayesian Tutorial.* Clarendon Press, Oxford., U.K.

STOKES, H.T., KISI, E.H., HATCH, D.M. & HOWARD, C.J. (2002): Group-theoretical analysis of octahedral tilting in ferroelectric perovskites. *Acta Crystallogr.* **B58**, 934-938.

SWAINSON, I.P. (2005): Tilt and acoustic instabilities in ABX_4, A_2BX_4 and ABX_3 perovskite structure type: their role in

the incommensurate phases of the organic-inorganic perovskites. *Acta Crystallogr.* **B61**, 616-626.

TAMAZYAN, R. & VAN SMAALEN, S. (2007): Quantitative description of the tilt of distorted octahedra in ABX$_3$ structures. *Acta Crystallogr*. **B63**, 190-200.

THOMAS, N.W. (1998): A new global parameterization of perovskite structures. *Acta Crystallogr*. **B54**, 585-599.

WOOD, I.G., KNIGHT, K.S., PRICE, G.D. & STUART, J.A. (2002): Thermal expansion and atomic displacement parameters of cubic KMgF$_3$ perovskite determined by high-resolution neutron powder diffraction. *J. Appl. Crystallogr*. **35**, 291-295.

ZHANG, ZHAOMING, HOWARD, C.J., KENNEDY, B.J., KNIGHT, K.S. & ZHOU, QINGDI (2007b): Crystal structure of *Ln*$_{1/3}$ NbO$_3$ (*Ln* = Nd, Pr) and phase transition in Nd$_{1/3}$NbO$_3$. *J. Solid State Chem*. **180**, 1846-1851.

ZHANG, ZHAOMING, HOWARD, C.J., KNIGHT, K.S. & LUMPKIN, G.R. (2006): Structures of the cation-deficient perovskite Nd$_{0.7}$Ti$_{0.9}$Al$_{0.1}$O$_3$ from high-resolution neutron powder diffraction in combination with group-theoretical analysis. *Acta Crystallogr*. **B62**, 60-67.

ZHANG, ZHAOMING, LUMPKIN, G.R., HOWARD, C.J., KNIGHT, K.S., WHITTLE, K.R. & OSAKA, K. (2007a): Structures and phase diagram for the system CaTiO$_3$–La$_{2/3}$TiO$_3$. *J. Solid State Chem*. **180**, 1083- 1092.